



אוניברסיטת בן-גוריון בנגב
Ben-Gurion University
of the Negev

הפקולטה למדעי הטבע
The Faculty of Natural Sciences
המחלקה למדעי הגיאולוגיה והסביבה
Department of Geological &
Environmental Sciences

Rockbursts simulations with the numerical DDA method

Thesis submitted in partial fulfillment

of the requirements for the

MASTER OF SCIENCES DEGREE

by

Ravit Zelig

Under the supervision of Prof. Yossef H. Hatzor

OCTOBER 2015

BEN- GURION UNIVERSITY OF THE NEGEV
THE FACULTY OF NATURAL SCIENCES
DEPARTMENT OF GEOLOGICAL & ENVIRONMENTAL SCIENCES

Rockbursts simulations with the numerical DDA method

Thesis submitted in partial fulfillment of the requirements for the

MASTER OF SCIENCES DEGREE

by Ravit Zelig

Under the supervision of Prof. Yossef H. Hatzor

Signature of student: _____ Date: _____

Signature of supervisor: Y. Hatzor. _____ Date: _____

Signature of chairperson

Of the committee for graduate studies: _____ Date: _____

OCTOBER 2015

Acknowledgment

I would like to thank my thesis advisor Professor Yossef H. Hatzor, for his support and guidance through this research and my academic studies.

Prop. Feng and his team from the Chinese Academy of Sciences, for the collaboration and the monitoring data from the Jinping II Hydropower Project.

Also my sincere gratitude to predecessor in developing the DDA method, your excellent work and willingness to help are very appreciated; Gony Yadoga-Biran, Yuval tal, and Huirong Bao.

It has been a great pleasure to study and work in the Department of Geological and Environmental Sciences, BGU. Especially to the administrative staff Rivka Eini and Zahla Sharabi for their assistant and availability to help with any occurring problem.

Of course, to my friends and fellow graduate student who was there to support, encourage, talk and open their house whenever needed; Tal Zaslavski, Maayan Shviro, Nir Badt, Omri Shitrit, Guy Tzur, and Neta Ginsburg.

And last, but not least a to my family who was there all the way to hold my hand through it all.

Table of Contents

Chapter 1 - Introduction	1
Chapter 2 - Research Method	4
2.1 The Discontinuous Deformation Analysis (DDA) method	4
2.1.1 DDA concepts	4
2.1.2 The DDA formulation	5
2.1.3 Block system kinematics and contacts	7
2.1.4 User-defined numerical control parameters in DDA	8
2.2 DDA modifications and improvements	9
2.2.1 The new viscous boundary condition in the DDA method	10
2.2.2 Excavation sequence in DDA method	11
2.3 Mesh construction using AutoCAD software	12
Chapter 3 - Simulating one dimensional P-wave propagation with DDA	14
3.1 Model geometry and mechanical properties.....	15
3.2 Analytical vs. DDA solution	16
3.3 DDA accuracy considering block length and time step size	18
Chapter 4 - Blast shock simulation with DDA	20
4.1 Model geometry.....	21
4.2 Results.....	23
4.3 Discussion	25
Chapter 5 - Validating shock-wave modeling with DDA using the Jinping case study..	28
5.1 Jinping II Hydropower Station as a case study.....	28
5.2 Model geometry for validation study.....	29
5.3 Result	32
5.4 Discussion	33
Chapter 6 - Strain Rockbursts Simulations with DDA.....	34
6.1 Strain relaxation mechanism for rockburst generation	37
6.1.1 Model assumptions	37
6.1.2 Simulation result.....	38
6.1.3 The role of initial stresses	41

6.2 Energy redistribution mechanism for rockburst generation	43
6.2.1 Model assumptions	43
6.2.2 Simulations results.....	45
6.2.3 The effects of the friction angle and the initial stresses.....	49
Chapter 7 - Summary and conclusions	52
Bibliography	53
Appendix A.....	59

List of Figures

FIGURE 2.1 - TYPES OF BLOCK CONTACTS: A) ANGLE TO EDGE. B) ANGLE TO ANGLE. C) EDGE TO EDGE (SHI ,1993).....	8
FIGURE 2.2 - DDA MECHANICAL BEHAVIOR DURING CONTACT: (A) NORMAL CONTACT AND (B) SHEAR CONTACT (WU ET AL. ,2004).....	8
FIGURE 2.3 A FLOW CHART DESCRIBING THE PROCEDURE OF MESH CONSTRUCTION USING AUTOCAD IN 2D-DDA.	13
FIGURE 3.1- THE CONFIGURATION OF THE MODELED ELASTIC BAR WITH DIFFERENT BLOCK LENGTHS	15
FIGURE 3.2- σ_x MEASURED 50 M FROM THE LOAD POINT WITH TIME STEP THE SIZE OF 10^{-4} s	17
FIGURE 3.3- σ_x MEASURED 50 M FROM THE LOAD POINT WITH TIME STEP THE SIZE OF 10^{-5} s.	17
FIGURE 3.4- COMPARISON BETWEEN THE STRESS AMPLITUDE ERROR FOR TWO DIFFERENT TIME STEP SIZES. THE DASHED LINE DELINEATES $H=1/12$	19
FIGURE 3.5- VELOCITY ERRORS AS A FUNCTION OF BLOCK (ELEMENT) LENGTH FOR TWO TIME STEP SIZES. THE DASHED LINE DELINEATES $H=1/12$	19
FIGURE 4.1- EXPLOSIVE PRESSURE TIME HISTORY. P_0 IS THE MAXIMUM PRESSURE, THE RED LINE IS THE SIMPLIFIED FUNCTION USED AS INPUT FOR DDA MODIFIED AFTER LOW (2001).	21
FIGURE 4.2- THE BLAST LOAD FUNCTION USED AS INPUT IN EVERY LOADING POINT AROUND OUR DDA BLAST MODEL	22
FIGURE 4.3- THE DDA BLAST MODEL USED IN THIS STUDY.....	22
FIGURE 4.4- THE CONFIGURATION OF THE BLAST MODEL, WITH A NON-REFLECTIVE BOUNDARIES AT THE BOUNDARIES OF THE MODELED DOMAIN AND POSITION OF MEASUREMENT POINTS IN THE HORIZONTAL (H) AND VERTICAL (V) DIRECTIONS.	23
FIGURE 4.5 - HORIZONTAL STRESS HISTORY +/- 0.1 S FROM BLAST.	24
FIGURE 4.6 - VERTICAL STRESS HISTORY +/- 0.1 S FROM BLAST.	24
FIGURE 4.7 - VELOCITY TIME HISTORY IN THE HORIZONTAL DIRECTION. THE BLAST ACCRUED AT 2 SECONDS.....	26
FIGURE 4.8 - VELOCITY TIME HISTORY IN THE VERTICAL DIRECTION. THE BLAST OCCURRED AT 2 SECONDS.	26
FIGURE 5.1 LOCATION AND PLAN OF THE JINPING II HYDROPOWER STATION: (A) LOCATION OF THE JINPING PROJECT IN CHINA, (B) LAYOUT OF THE JINPING HYDROPOWER PROJECT ACROSS THE YALONG RIVER, (C) CONFIGURATION OF SEVEN TUNNELS (LI ET AL. ,2012).....	29
FIGURE 5.2 - DIAGRAM SHOWING MS MONITORING IN THE TUNNEL (FENG ET AL. ,2015).....	30
FIGURE 5.3 – THE DDA MODEL OF THE MONITORED TUNNEL SEGMENT AT JINPING WITH LOCATION OF MEASUREMENT POINTS USED FOR VALIDATION.	31
FIGURE 5.4- PRINCIPAL STRESS TRAJECTORIES IN THE MODELED DOMAIN AT THE END OF THE SIMULATION.	32
FIGURE 5.5- VELOCITY TIME HISTORY IN THE HORIZONTAL DIRECTION (BLUE LINE), THEORETICAL ARRIVAL TIMES OF SHOCK WAVE (RED TRIANGLES), AND ARRIVAL TIME IN MONITORED POINTS IN THE FIELD (*).	33
FIGURE 6.1 EJECTION-TYPE ROCKBURST RESULTS FROM EXPULSION OF JOINT OR FRACTURE-DEFINED BLOCK OF ROCK. (ORTLEPP & STACEY ,1994).....	34
FIGURE 6.2- DDA MESH OF ANALYZED DOMAIN COUPPLIED WITH AUTOCAD PREPROCESSING.....	38
FIGURE 6.3- AXIAL STRESS IN MEASUREMENT POINT (MP) 3 AND 5.....	39

FIGURE 6.4- THE RESULT OF THE STRAIN-RELAXATION SIMULATIONS FOR INITIAL STRESSES OF (A) 0 MPA ,(B) 10 MPA, (C) 30 MPA, (D) 50 MPA.	40
FIGURE 6.5- THE RELATION BETWEEN THE INITIAL STRESS OF THE ROCK MASS AND THE VELOCITY (A) AND ACCELERATION (B) OF THE EJECTED KEY BLOCK (NO. 1) IN RESPONSE TO THE EXCAVATION INDUCED STRAIN RELAXATION.	42
FIGURE 6.6- THE SIMULATED DDA MODEL	44
FIGURE 6.7- MODEL LAYOUT WITH DIMENSIONS AND MEASUREMENT POINT LOCATIONS.....	44
FIGURE 6.8 – PRINCIPAL STRESS TRAJECTORIES AT THE END OF THE DDA SIMULATION WITH NO INITIAL STRESSES WITH JOINT FRICTION ANGLE OF A) 0°, B) 5°, C) 15°, D) 25°, E) 35°, F) 45°.	46
FIGURE 6.9 - PRINCIPAL STRESS TRAJECTORIES AT THE END OF THE SIMULATION WITH INITIAL HYDROSTATIC STRESSES OF 50 MPA WITH JOINT FRICTION ANGLES OF A) 0°, B) 5°, C) 15°, D) 25°, E) 35°, F) 45°.....	47
FIGURE 6.10 – PEAK STRESS RECORDED IN THE CONTROL POINT 5 AND 6 (A) WITHOUT INITIAL STRESS (B) WITH INITIAL HYDRO STRESS OF -50 MPA.....	48
FIGURE 6.11- PEAK VELOCITY (A) AND PEAK ACCELERATION (B) AROUND THE TUNNEL WITH (LEFT) AND WITHOUT (RIGHT) INITIAL STRESSES.	50
FIGURE 6.12- PEAK VELOCITY (A) AND PEAK ACCELERATION (B) OF KEY-BLOCK 1 WITH INITIAL HYDROSTATIC STRESS OF 0 MPA (BLUE CIRCLES) AND 50 MPA (GREEN TRIANGLES).....	51

List of Tables

TABLE 3.1: INPUT PARAMETERS USED IN WAVE PROPAGATION THROUGH ELASTIC BAR SIMULATIONS	16
TABLE 3.2: CONCENTRATED STRESS ACCURACY RESULTS FOR P WAVE PROPAGATION THROUGH ELASTIC BAR	18
TABLE 3.3: CONCENTRATED VELOCITY ACCURACY RESULTS FOR P WAVE PROPAGATION THROUGH ELASTIC BAR.	18
TABLE 4.1: PEAK ARRIVAL TIME ERRORS IN THE DIFFERENT MEASURMENT POINTS.	27
TABLE 5.1: COORDINATES OF SENSOR IN THE TUNNEL.....	30
TABLE 5.2: ROCK PROPERTIES AT THE STUDIED SECTION OF THE JINPING HYDROPOWER PROJECT (TUNNEL F) FOLLOWING RESULTS PUBLISHED BY LI ET AL. (2012).	31
TABLE 6.1: ROCK MESH PROPERTIES:	37
TABLE 6.2: INPUT PARAMETERS FOR DDA.	43

Abstract

Rock-bursts can be defined as a sudden displacement of rock in deep excavations that can come in different intensities and may cause severe damage in life and equipment. Two source mechanisms are typically considered for rock-bursts: 1) Strain relaxation leading to displacement of excavation surfaces, 2) Energy redistribution induced by explosions and drilling activity at the working face. In this study, we investigate further into those mechanisms using the numerical Discontinuous Deformation Analysis (DDA) method.

DDA is a numerical, discrete element method, which solves a more general type of a finite element mesh. By using a new viscous boundary and excavation sequence modeling capabilities we now have the ability to model dynamic deformation during deep tunneling excavations at higher accuracy. The rock-burst type considered here is slip-fault based, we assume that before intact rock strength will be exceeded by excavation-induced stress concentrations, existing key blocks will be ejected in response to tunneling due to the much lower shear strength of the discontinuities when compared to shear strength of intact rock.

To verify the accuracy of the DDA wave propagation in a discontinuous medium, a simulation of P-wave in one-dimension elastic bar was performed. The results show that DDA presents high accuracy provided that the time step is sufficiently small and the ratio between block and wave lengths is between $1/8$ and $1/12$. Additionally, a radial P-wave propagation simulation was formed to emulate an underground blast. Finally, a simulation of a blast functioning as a micro seismic event in a discontinuous medium with an open tunnel was compared to in-situ measurements made in the Jinping II Hydropower project in China.

After performing the validations successfully, we study two possible rock burst generation mechanisms: 1) due to strain relaxation as response to opening in various in situ stresses environments [0-50 MPa], and 2) due to nearby blasting with different friction angle and in situ stresses. A very strong relation between the initial stress and the velocity and acceleration of the ejected key blocks following the removal of the tunnel section is reported. We also find that the influence of blasting on rock burst phenomena is strongly related to the initial in situ stress level. We conclude that under relatively low in situ stress environments nearby blasting may indeed ejection of originally stable key

blocks. However, under high in situ stress conditions strain relaxation poses a much greater rock-burst risk.

Chapter 1 - Introduction

Rockbursts pose a very serious risk to the safety of deep underground excavations, and yet the underlying mechanism for their generation is still not completely understood. Because of the great risk to workers safety and the extensive damage to equipment, rockbursts are considered by many as the most significant unresolved challenge in deep underground excavations. As this term may have many definitions, we define it as a “sudden displacement of rock that occurs at the boundary of an excavation and causes substantial damage to the excavation” (Brady & Brown ,2007). Rockbursts usually occur during excavation of underground space in the form of rock slices or falls, or ejection of rock fragments, sometimes accompanied by cracking sounds.

At present, two basic mechanisms are discussed in the rock mechanics literature: 1) Strain relaxation that leads to the displacement of excavation surfaces, in which case the source and damage are concurrent; and 2) Seismic wave propagation from energy redistribution that is induced by explosions and drilling in the excavation, in which case the source and the damage might be separated in distance and time (Ortlepp & Stacey ,1994). Typically, deep excavations can release an immense amount of accumulated elastic energy accompanied with intensive dynamic loading (Cook ,1966). The stored strain energy in the rock mass cannot be dissipated entirely by shear sliding along joints, and part of the released strain energy may be converted into kinetic energy, leading to strong shock coupled with block ejections.

In considering global tunnel and underground space stability, the main concern is comprehensive control of rock mass displacement throughout the near-field domain of the underground space. Underground tunneling disturbs the equilibrium of the surrounding rock and leads to stress redistribution (Gu & Ozbay ,2014). Rockbursts are mostly associated with hard rocks and geological structures such as faults and dykes, and in excavations are often related to high extraction ratios and associated with tunneling methods causing unfavorable stress conditions (Kaiser & Cai ,2012). Assurance of underground space global stability must be based on the principles of stability of equilibrium well known in basic engineering mechanics. Essentially, the requirement is

to make sure that any small change in the equilibrium state of loading in a structure cannot provoke a sudden release of energy or large change in the geometry of the structure.

The complexity of rockbursts is in the prediction of an individual event. Former research has shown that their occurrence is dependent on many factors such as excavation methods, geological structures, *in-situ* stress conditions, rock mass strength, and the size of excavation (Mansurov ,2001; Wang & Park ,2001; Lee et al. ,2004). In the past several decades, extensive research related to the mechanism of rockbursts has been performed. *In-situ* measurements of rock displacement in deep tunneling projects since the 1960's suggest that the mechanical response of the rock mass in rockbursts events is essentially elastic in nature (Mitri ,1999). Generally, rockbursts fall under one of three classifications: 1) strain bursts, 2) pillar burst, and 3) fault slip burst (Müller ,1991). In civil works, the most common phenomena are referred to as strain bursts, although buckling and face crushing may occur as well (He et al. ,2015). As pointed out, rockbursts are a violent failure phenomenon associated with a seismic event, which often occurs in deep, highly stressed ground (Kaiser et al. ,1996), the response of which cannot be addressed by static theories of rock behavior. Consequently, a deeper insight into the dynamic mechanisms and the application of this knowledge to the excavation and support of underground openings is essential for the possible reduction of the risk associated with the rockbursts phenomenon (Durrheim et al. ,1998). To date, the rockburst phenomenon been studied in the field using *in-situ* microseismic monitoring, at the lab using true triaxial tests, and theoretically using analytical and numerical approaches.

In-situ monitoring of micro seismicity has been conducted in various projects, in America (Brady & Leighton ,1977), South Africa (Ortlepp & Stacey ,1994), Canada (Kaiser & Maloney ,1997), India (Srinivasan et al. ,1997), Australia (Heal ,2010), and China (Feng et al. ,2012; Lu et al. ,2013), in an effort to understand spatial and temporal intensities of rockburst events during underground mining. Interestingly, spatial precursor events were determined a few days before the occurrence of major rockbursts. Moreover, micro-seismicity monitoring enabled resolving the moment tensor associated with rockbursting to analyze their shearing mechanism of rockbursts (Cai et al. ,2004).

Laboratory dynamic unloading tests under true triaxial conditions were performed to obtain the frequency amplitude relationship of acoustic emissions resulting from rockbursts of a single rock block (He et al., 2015; Zhao et al., 2014). Analysis of such laboratory induced “strain-bursts” in granitic rocks revealed that strain-bursts are non-linear, dynamic phenomena that occur when a large amount of energy is released towards a pre-existing free face by sliding along pre-existing discontinuities. Through triaxial unloading tests, it was found that the unloading elastic modulus is lower than under loading, and that the ultimate strength decreases with the increasing rate of unloading (Huang et al. ,2001).

The mechanism of rockbursts triggered by the release of finite key blocks (Goodman & Shi ,1985), formed in the rock mass by intersection of pre-existing joints, needs to be better understood for the optimization design of support and safety operation of mining and underground engineering. It is to be expected that given strong strain relaxation, removable key blocks will be ejected from the rock mass into the newly formed space before intact rock elements experience fracturing induced by stress concentrations because of the much lower shear resistance of discontinuities with respect to the shear strength of intact rock. This rationale provides the motivation to focus the numerical analysis in this study on discrete element methods, and we have chosen to do this with the numerical, implicit, discontinuous deformation analysis method (DDA) (Shi, 1993).

Chapter 2 - Research Method

2.1 The Discontinuous Deformation Analysis (DDA) method

The DDA method is briefly described in this chapter, and some recently introduced enhancements to DDA that are used extensively in this research are discussed.

2.1.1 DDA concepts

The Discontinuous Deformation Analysis (DDA) is a numerical, discrete element method (DEM) that originated in a back-analysis algorithm to determine the best fit for a deformed configuration of a block system from measured displacements and deformations (Shi & Goodman ,1985). DDA was then further developed to perform the complete deformation analysis of a block system (Shi ,1988). The DDA method parallels the finite element method, which uses standard finite element method (FEM) meshes over isolated blocks bounded by pre-existing discontinuities. However, DDA is more general, where blocks can be of any convex or concave shape, as well as multi-connected polygons with holes.

The DDA method simulates a system of individually deformable blocks that move independently with minimal interpenetration. The formulation of DDA is based on dynamic equilibrium that considers the kinematics of individual blocks, as well as the friction along the block interface. The equilibrium equations are derived by minimizing the total potential energy of the block system, and the unknowns of this formulation are the displacement and deformation of the blocks, or element. The method automatically identifies contacts between blocks and applies numerical penalties to the contacts in the form of rigid springs. In each time step, all contacts are checked by enforcing a “no tension-no penetration” criterion with an “open–closed” iteration procedure that is unique to DDA. Friction between the blocks is implemented by means of the Mohr-Coulomb failure criterion. The solution is performed according to a time step marching scheme. The DDA method has emerged as an attractive model for geo-mechanical problems

because its advantages cannot be replaced by continuum-based methods or by explicit DEM formulations.

2.1.2 The DDA formulation

In the DDA the displacement at any point in block i , in a system that consists of n blocks, is represented by vector d_i , which contains six displacement variables:

$$d_i = \{u_0 \quad v_0 \quad r_0 \quad \varepsilon_x \quad \varepsilon_y \quad \gamma_{xy}\}_i^T, \quad (i = 1, 2, \dots, n) \quad (1)$$

where (u_0, v_0) represent the displacement components (u, v) of a specific point (x, y) on the block i , and r_0 represents the rotation angle of the block with a rotation center at (x_0, y_0) , r_0 is given in radians. For a two-dimensional formation of DDA, the center of rotation (x_0, y_0) coincides with a block centroid (x_c, y_c) . The $[\varepsilon_x \quad \varepsilon_y \quad \gamma_{xy}]$ components represent the normal and shear strains of the block. Shi (1988) showed that the complete first order approximation of block displacement takes the following form

$$\begin{pmatrix} u \\ v \end{pmatrix}_i = [T_i][d_i] \quad (i = 1, 2, \dots, n) \quad (2)$$

where:

$$T_i = \begin{bmatrix} 1 & 0 & -(y - y_0) & (x - x_0) & 0 & (y - y_0)/2 \\ 0 & 1 & (x - x_0) & 0 & (y - y_0) & (x - x_0)/2 \end{bmatrix}_i \quad (3)$$

When combining Eq. (2) and Eq.(3), the complete first order approximation can be rewritten as:

$$\begin{pmatrix} u \\ v \end{pmatrix}_i = \begin{pmatrix} 1 & 0 & -(y - y_0) & (x - x_0) & 0 & (y - y_0)/2 \\ 0 & 1 & (x - x_0) & 0 & (y - y_0) & (x - x_0)/2 \end{pmatrix}_i \begin{pmatrix} u_0 \\ v_0 \\ r_0 \\ \varepsilon_x \\ \varepsilon_y \\ \gamma_{xy} \end{pmatrix}_i \quad (4)$$

This equation enables the calculation of displacements at any point (x, y) of the block when the displacements are given at the center of rotation and when strains are known. It assumes that the stresses and strains are constant in every block. This might limit the accuracy of the DDA method when dealing with wave propagation problems (a limitation that will be discussed later on).

For the calculation of the acceleration and the velocity of a block, we assume that the initial velocity at the beginning of the time step is \dot{d}_o , a value that can be obtained from the last time step, and that the time interval for a single time step is t . Thus, the equations of motion would be:

$$\begin{cases} \dot{d} = \frac{2d}{t} - \dot{d}_o \\ \ddot{d} = \frac{2}{t^2}(d - t\dot{d}_o) \end{cases} \quad (5)$$

The simultaneous equilibrium equations can be written as follows:

$$M\ddot{d} + C\dot{d} + Kd = f \quad (6)$$

where M, C and K are the mass matrices, damping matrices and stiffness matrices, respectively, d is the unknowns vector, and f is the force vector. By substituting Eq. (5) with the simultaneous equations, Eq. (6) can be rewritten as:

$$\widehat{K}d = f \quad (7)$$

Where \widehat{K} is the equivalent global stiffness matrices, and Eq. (7) can be written in the sub matrices form:

$$\begin{bmatrix} K_{11} & K_{12} & K_{13} & \dots & K_{1N} \\ K_{21} & K_{22} & K_{23} & \dots & K_{2N} \\ K_{31} & K_{32} & K_{33} & \dots & K_{3N} \\ \vdots & \vdots & \vdots & \ddots & \vdots \\ K_{N1} & K_{N2} & K_{N3} & \dots & K_{NN} \end{bmatrix} \begin{Bmatrix} d_1 \\ d_2 \\ d_3 \\ \vdots \\ d_n \end{Bmatrix} = \begin{Bmatrix} f_1 \\ f_2 \\ f_3 \\ \vdots \\ f_n \end{Bmatrix} \quad (8)$$

where K_{ij} elements form a 6×6 sub-matrices that defined by the material properties of block i . d_i and f_i are 6×1 sub-matrices, where the first matrices represents the deformation variables of block i and the second matrices represents the load on block i that is distributed to the six deformation variables. In the off diagonal sub-matrices $K_{ij(i \neq j)}$ the stiffness is defined by the contacts between block i and block j and other inter-element actions such as bolting. The diagonal sub-matrices $K_{ij(i=j)}$ represents the sum of the contributing sub-matrices for the i^{th} block, namely block inertia and elastic strain energy.

The equilibrium equations are derived by minimizing the total potential energy P produced by the forces and stresses. The i^{th} row of Eq. (8) consists of six linear equations:

$$\frac{\partial \Pi}{\partial d_{ri}} = 0, \quad r = 1, \dots, 6 \quad (9)$$

Where d_{r_i} represents the deformation variables of block i . The total potential energy Π is the summation over all potential energy sources.

2.1.3 Block system kinematics and contacts

Block system kinematics in DDA is mathematically described by a system of inequalities constrained by the no-tension no-penetration condition between the blocks. As pointed out, the minimization of total potential energy with inequality constraints is a non-linear programming problem of high difficulty. However, the block system moving or deforming the blocks is in contact only along boundaries, and the non-penetration inequalities can be transformed into equations when the blocks are in contact.

The equations can be imposed on the global equation by adding numeric penalties to lock the movement in one or two directions. If two blocks have a tensile contact force between them, they will separate when the locks are removed, and the global equation has to be solved repeatedly while selecting the lock position by iterations. Using this method, the block system with tension and penetration can be corrected, by selection of lock positions, until the fundamental constraints are satisfied.

In DDA, there are three types of block contacts: edge-to-edge, vertex-to-vertex, and vertex-to-edge. An edge-to-edge contact can be transformed into two vertex-to-edge contact candidates; Vertex P_1 to Edge P_3P_4 and Vertex P_4 to Edge $P_1 P_2$ (see Figure 2.1). When contacts occur, contact forces are applied through contact springs with a stiffness k_n in the normal direction and a stiffness k_s or frictional force in the tangential one, as shown in Figure 2.2. The contact forces are disregarded when blocks separate. When the shear force is smaller than the shear strength of the joint, the shear contact spring is applied to reduce the relative tangential displacement. Once the shear force is larger than the shear strength, the slider dominates the shear behavior instead of the shear spring. DDA uses the Updated Lagrange description to calculate the large displacements of blocks step-by-step.

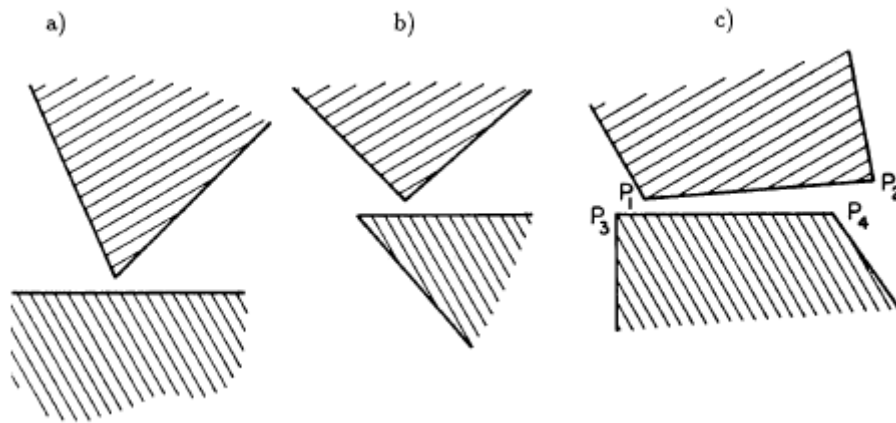


Figure 2.1 - Types of block contacts: a) angle to edge. b) angle to angle. c) edge to edge (Shi ,1993).

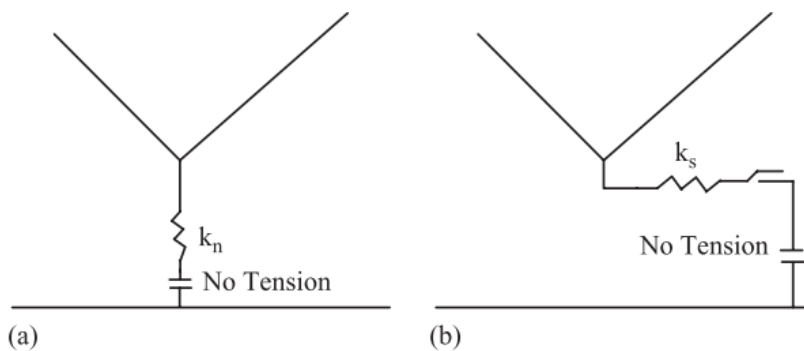


Figure 2.2 - DDA mechanical behavior during contact: (a) normal contact and (b) shear contact (Wu et al. ,2004).

2.1.4 User-defined numerical control parameters in DDA

The DDA used in this research is an advanced version of the original code developed by Shi (1993). The numerical control parameters required to defined for input in DDA are:

k01- the dynamic control parameter. For a fully static analysis, where the velocity is zeroed at the beginning of each time step, a value of 0 is entered. For a fully dynamic analysis where the velocity at the beginning of a time step is fully inherited from the velocity at the end of the previous time step, a value of 1 is entered. Any number between 0 to 1 corresponds to a measure of kinetic damping or energy dissipation in the analysis, i.e. $k01=0.97$ means a 3% velocity decrease from the end of a time step to the beginning of the next. This parameter can be used as proxy for damping effects.

g_0 – the contact spring stiffness, also expressed as “ k ”, in order to minimize penetration and tension. The g_0 is a parameter that has a large effect on the result of the analysis; therefore, it must be selected carefully. If possible, it should be selected by comparing the DDA results to an existing analytical solution, and performing iterations until a satisfying agreement is obtained. According to the DDA user manual (Shi ,1996), a suitable value for g_0 is $E \times L$, where E is Young’s modulus and L is the average diameter of a block in the analyzed domain.

g_1 -the time step interval. This number should be small enough to guarantee infinitesimal displacements at each time step. Attentive and educated selection of the g_1 value will ensure both high efficiency and high accuracy of the numerical solution.

g_2 - the assumed maximum displacement per time step ratio, a dimensionless quantity related to the size of the model. It is used to find possible contacts between blocks, and it should be small enough to secure infinitesimal displacements at each time step, and to ensure the convergence of the solution.

2.2 DDA modifications and improvements

As science has evolved through the years, the DDA method also has developed. Since its first publication in 1988, many modifications and developments have been introduced including more accurate stress-deformation analysis, for example (Shyu ,1993; Chang ,1994), and for coupled stress-flow problems (Jing et al. ,2001; Kim et al. ,1999). With this more extensions and improvements have been implemented over the years, with the bulk of the publications appearing in a series of ICADD conferences. The code development has reached a certain level of maturity with applications focusing mainly on tunneling (Yeung & Leong ,1997), slope failure (Chen ,2003), failure behavior of joints like fracturing and fragmentation processes of geological and structural materials (Lin et al. ,1996; Zhang et al. ,2014; Pearce et al. ,2000) and earthquake effects (Hsiung & Shi ,2001). In this research, we will focus on developments that has improved modeling wave propagation and tunneling with the DDA.

2.2.1 The new viscous boundary condition in the DDA method

In order to simulate the infinite domain with a finite model, a dynamic analysis with non-reflective boundary conditions is advantageous, as stiff model boundaries might trigger artificial wave reflections that will inevitably impair the numerical solution.

The global stiffness matrices $[K]$ is obtained by assembling different sub-matrices, and each sub-matrices can be derived from its corresponding potential energy formulae. Bao et al. (2012) showed how a viscous boundary could be implemented using an analytical solution proposed by Lysmer and Kuhlemeyer (1973).

The viscous boundary model in the DDA method is based on a system of dashpots that are positioned at any selected domain boundary. These dashpots are capable of damping out most of the reflections by using the equations that were originally proposed by Lysmer and Kuhlemeyer (1973) for wave propagation analysis in a porous media. Bao et al. (2012) incorporated these boundary equations into the DDA method, and demonstrated the high absorbing efficiency that has been obtained.

This viscous boundary sub-matrices they developed, consists of the derivatives of the potential energy components that are stored in the boundary dashpot. The potential energy in a dashpot must equal the work of the reacting force in the dashpot for each single time step. Therefore, the viscous force from the dashpot is assumed proportional to the velocity of the dashpot at the attaching point.

The non-reflective boundary enhancement proposed by Bao et al. (2012) involves dampers in the normal and tangential directions, which incorporate the block velocities:

$$\begin{cases} f_n = -\rho c_p v_n \\ f_s = -\rho c_s v_s \end{cases} \quad (10)$$

Where ρ is material density, c_p and c_s are the characteristic propagation velocities of P and S -waves in the material, and v_n and v_s are the normal and tangential velocities of the boundary block. From elastic wave propagation theory, the characteristic P and S -wave velocities for the material are:

$$c_p = \sqrt{\frac{E(1-\nu)}{\rho(1+\nu)(1-2\nu)}} \quad (11)$$

$$c_s = \sqrt{\frac{E}{\rho(1+\nu)}} \quad (12)$$

Where ρ is material density, E , ν are the material's Young's modulus and Poisson's ratio, respectively.

The normal and tangential particle velocities of the boundary in Cartesian coordinates can be obtained by the following transformation:

$$\begin{cases} v_n = v_x \sin \alpha - v_y \cos \alpha \\ v_t = v_x \cos \alpha + v_y \sin \alpha \end{cases} \quad (13)$$

Where α is the direction angle of the boundary edge corresponding to the x -axis; v_x and v_y are the block velocities in the x and y directions, respectively.

2.2.2 Excavation sequence in DDA method

To simulate the response of the rock mass to tunneling as accurately as possible we model the excavation sequence using a development that was originally introduced into the numerical manifold method by Tal et al. (2014). In the original DDA code, underground openings are modeled as an existing cavity in the mesh from the first time step and throughout the simulation. However it has been observed by many researchers that gravity is not immediately "turned on" in DDA (MacLaughlin & Sitar, 1999). Also the numerical values of the stresses at a given depth in the mesh approach the theoretical value only after a significant number of time steps have elapsed, the number of which has been shown to increase with the increasing number of blocks in the mesh (Hatzor et al. 2010). Naturally, the theoretically available frictional resistance across the discontinuities, defined by the assigned friction angle and the level of normal stress acting on the joints, is not fully mobilized until gravity is completely turned on and the stresses acting on the joints attain their ultimate magnitude. Consequently, blocks that are free to move from the rock mass into the excavation space from a kinematical stand point will tend to do so from the first time step of the simulation, when the frictional resistance

is much lower than the theoretical level. This will obviously lead to exaggerated block displacements and as a result to overly conservative design.

The original DDA code was modified by Yuval Tal while at BGU, following the work of Tal et al. (2014) on the numerical Manifold Method. The modification enables modeling tunnel excavation during the DDA simulation after the initial stresses are fully developed, and the corresponding elastic deformation has already taken place. The modified DDA code consists of two stages: (1) the simulation starts with a single or few blocks replacing the intentional tunnel excavation space, and “static” simulation is executed until equilibrium is attained. A “static” simulation means the initial velocity at the beginning of every time step is set to zero everywhere in the domain. Then, (2) to simulate the tunnel excavation, the intentional tunnel blocks are removed at once or step by step, and a “dynamic” or “static” computation is executed as requested at the start of the simulation. A “dynamic” simulation means the terminal velocity in the previous time step is inherited in the new time step everywhere in the domain. Instead of reducing the elastic constants (e.g. Young's modulus, Poisson's ratio) or assigning zero stress in all elements inside the tunnel during the excavation simulation as has been attempted by others, here, the tunnel elements are simply removed altogether. We choose to do this because numerical instabilities may occur when removable blocks, which are free to move from a kinematical standpoint, contact tunnel elements having zero or very minimal stiffness.

2.3 Mesh construction using AutoCAD software

The original DDA software package consists of four programs (Shi ,1996):

- 1) The line-producing program DDA Lines (dl) generates lines representing joints, the boundary of the joint domain, and perimeter tunnels. The lines representing joints can be generated statistically.
- 2) The block-producing program DDA Cut (dc), generates the block system by forming all possible blocks from individual line segments.
- 3) The analysis program DDA Forward (df), performs the DDA forward static or dynamic analysis of a block system. The system of simultaneous equation formulated in

DDA is solved by either a direct method with non-zero storage or a successive over-relaxation (SOR) iteration method.

4) The graphic output program DDA Graph (dg), is a graphic post-processor, which produces graphic output on the screen and produces postscript files for printing.

The AutoCAD comes handy in the process of the block cutting in a complex mesh, such as in masonry structures or discrete blocks formed in nature, because the DDA “dc” code does not have a graphic interface. For rock masses, that form by intersection of a systematic joint sets the dc is the simpler choice. Modeling multi-block structures in 2D-DDA here is based on augmentation made by Gony Yagoda-Biran (2013).

The steps for constructing a mesh in the 2D-DDA using AutoCAD are described briefly in Figure 2-3:

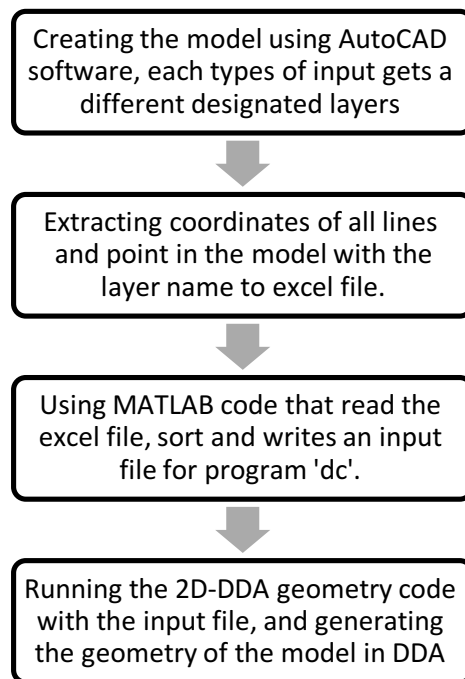


Figure 2.3 A flow chart describing the procedure of mesh construction using AutoCAD in 2D-DDA.

The MATLAB code that reads the Excel file, sorts, and writes an input file for program “dc” is provided in Appendix A.

Chapter 3 - Simulating one dimensional P-wave propagation with DDA

Even though the accuracy of numerical methods for solving wave propagations problems has been studied extensively, (Lysmer & Kuhlemeyer ,1973; Chen & Zhao ,1998; Van den Abeele et al. ,2007; Ainsworth & Wajid ,2009), in the attempt to calculate a wave propagation problem with numerical methods, it is difficult to obtain accurate results that are precisely equal to the analytical solutions because of numerical dissipation and dispersion phenomena. In linear static problems, the solutions obtained from the finite element method (FEM) converge to the exact solutions with mesh refinement, whereas the FEM solutions for linear elasto-dynamic problems may diverge due to mesh refinement and the use of small time increments. Moreover, when the problem consists of a rock mass with multiple fractures that often control the deformation.

The DDA method has emerged as an attractive model because of its intrinsic feature of block discontinuity at contact boundaries, as discussed. The longitudinal wave propagation in a one-dimensional bar is a simple case that may be used for validation and numerical calibration with respect to optimal numerical control parameters such as time step size and block (element) size. One of DDA assumption is that the stresses and strains are computed for the centroid of each block in the system using first-order approximation. Namely, there is no stress/strain distribution within the individual blocks, an assumption that may compromise solution accuracy. In order to overcome this limitation and to find the inner stresses within the bar, we divide the bar to blocks of equal lengths (see Figure 3.1) and analyze the effect of block size on the numerical errors in DDA.

The analytical solution for the P wave velocity as it propagates through a one dimensional elastic bar is given by the following formula (Kolsky ,1964):

$$V_p = \sqrt{\frac{E}{\rho_0}} \quad (14)$$

Where ρ_0 is the density of the rock and E is Young's modulus. The relative errors for the wave stress (amplitude) and the wave velocity are expressed as:

$$e = \frac{|A_1 - A_0|}{A_0} \times 100\% \quad (15)$$

Where A_1 is the measured wave amplitude or the calculated wave velocity at a reference measurement point in the model, and A_0 is the incident wave amplitude or analytical wave velocity at the same point.

In the study of Lysmer and Kuhlemeyer (1973) that was mentioned here earlier they also found that in order to obtain good accuracy the ratio between the block size and the wave length should be kept between 1/8 and 1/12, they labeled this ratio η :

$$\eta = \frac{\Delta x}{\lambda} \quad (16)$$

Where Δx is the size of the block and λ is the wave length.

3.1 Model geometry and mechanical properties

In order to test the effect of block size on numerical errors in the DDA method, five different block sizes were tested (0.5, 1, 2, 5, 10 m) in a 100 m long and 1 m wide elastic bar. The measuring point was positioned at 50 m from the left end of the bar (see Figure 3.1).

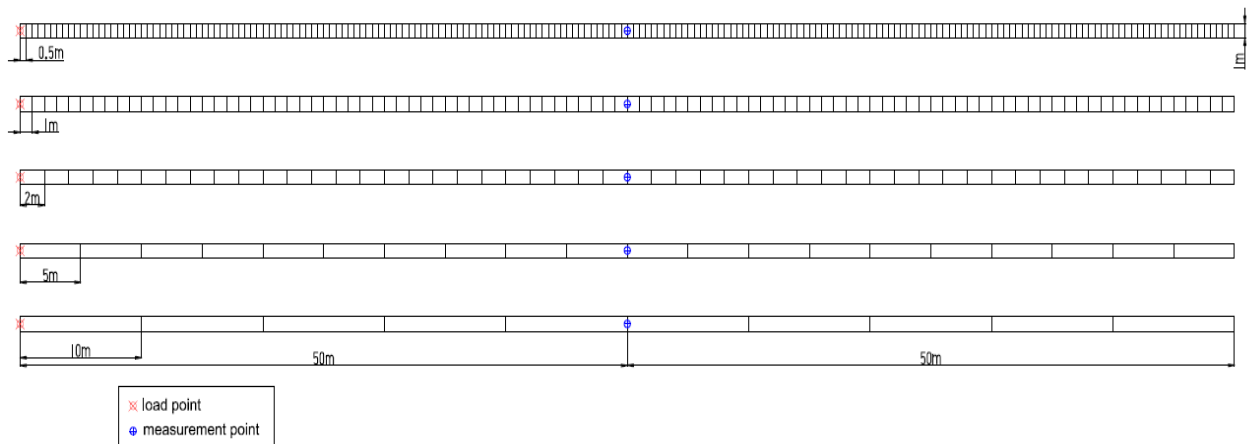


Figure 3.1- The configuration of the modeled elastic bar with different block lengths

The simulation is performed under zero gravity. The incident P wave is a one-cycle horizontal sinusoidal wave with frequency of 100 Hz, generated at a loading point positioned at the left end of the bar. The input horizontal load is described by:

$$F(t) = 1000 \sin(200\pi t) \text{ [KN]} \quad (17)$$

The material properties in the modeled bar are listed in Table 3.1.

Table 3.1: Input parameters used in wave propagation through elastic bar simulations

Density (kg/m³)	2650
Young's modulus (GPa)	50
Poisson ratio	0.25
Discontinuity friction angle (°)	35
Cohesion (MPa)	24
Tensile strength (MPa)	18

3.2 Analytical vs. DDA solution

The effect of the time step size on the numerical analysis was also tested in this study. Two different time step sizes were examined, 10^{-4} s and 10^{-5} s. Each time step size was tested with four different block length models. Figure 3.2 and Figure 3.3 show the σ_x stress measured at the measurement point, 50m from the load point, with a comparison to the analytical solution when the time step is 10^{-4} s and 10^{-5} s, respectively.

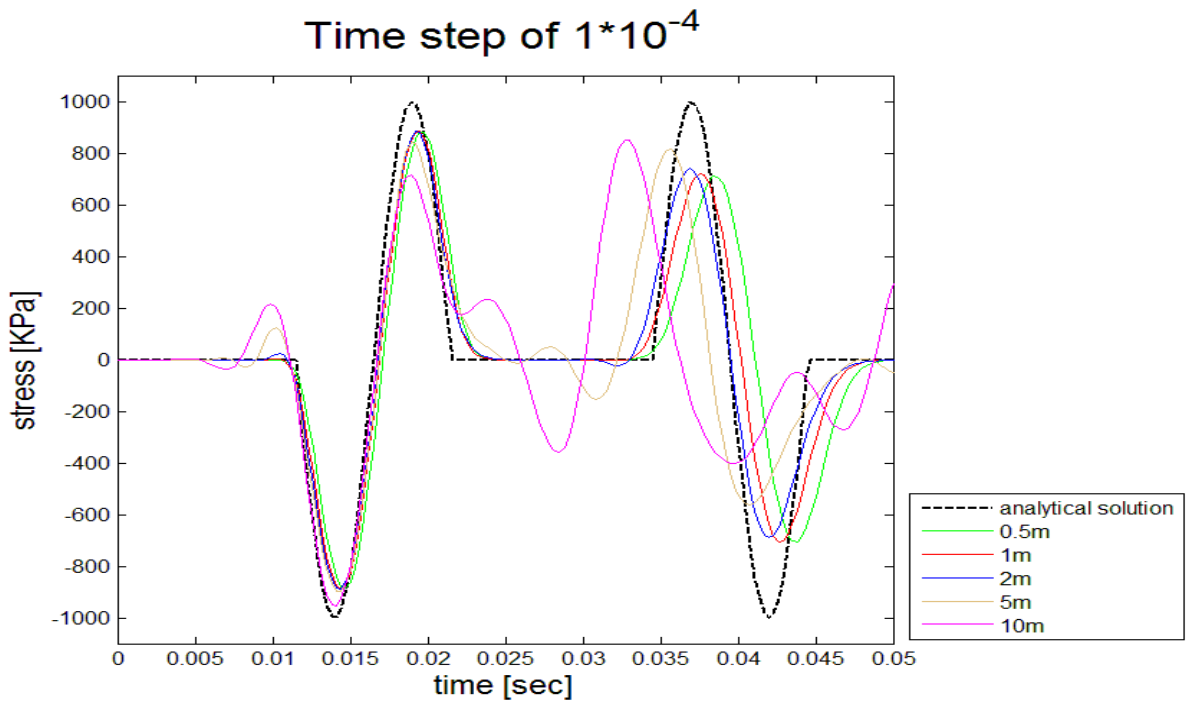


Figure 3.2- σ_x measured 50 m from the load point with time step the size of 10^{-4} s

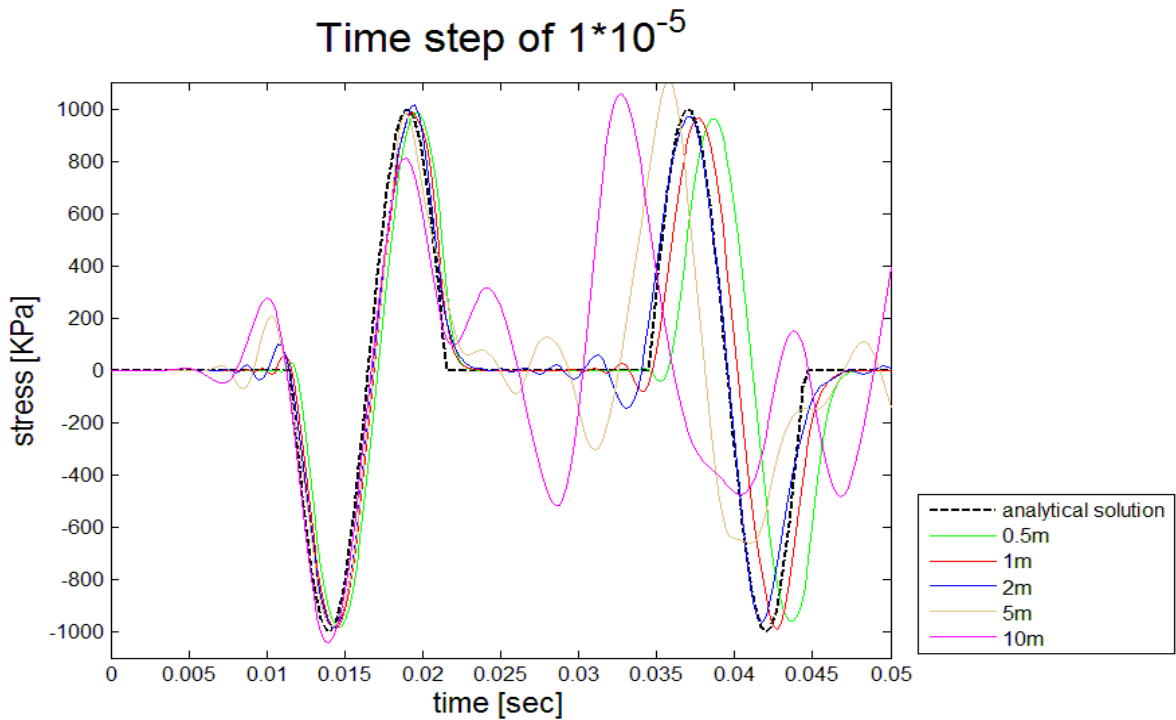


Figure 3.3- σ_x measured 50 m from the load point with time step the size of 10^{-5} s.

3.3 DDA accuracy considering block length and time step size

The relative errors with respect to velocity and stress are listed in Table 3.2

Table 3.3

Table 3.2: Concentrated stress accuracy results for P wave propagation through elastic bar

Δt (ms)	block length (m)	0.5	1	2	5	10
	$\eta (\Delta x/\lambda)$	0.012	0.023	0.046	0.115	0.230
0.01	amplitude (KPa)	983.6	985.4	999.8	981.6	927.5
	error	1.6%	1.5%	0.0%	1.8%	7.2%
0.1	amplitude (KPa)	884.6	887.3	888.2	870.3	835.3
	error	11.5%	11.3%	11.2%	13.0%	16.5%

Table 3.3: Concentrated velocity accuracy results for P wave propagation through elastic bar.

Δt (ms)	block length (m)	0.5	1	2	5	10
	$\eta (\Delta x/\lambda)$	0.012	0.023	0.046	0.115	0.230
0.01	velocity (m/s)	4219.16	4310.34	4359.20	4436.36	4432.43
	error	2.87%	0.77%	0.36%	2.13%	2.04%
0.1	velocity (m/s)	4884.24	4699.91	4553.73	4493.57	4490.35
	error	12%	8%	5%	3%	3%

Results for the one-dimension wave propagation problem through an elastic bar suggest that the DDA method can provide good accuracy with a relative error of less than 2%, depending on the numerical control parameters (time step size and block length). The results obtained here are consistent with the optimal ratio of η as suggested by Lysmer & Kuhlemeyer (1973) as shown in Figure 3.4 and Figure 3.5. It is also detectable that as the size of the blocks decreases, the relative error increases. Clearly for a fixed bar length reducing the block length increases the number of blocks in the beam, thus increasing the numerical penalties (number of contact springs), and, consequentially, the relative error. Another factor affecting DDA accuracy is the first-order approximation whereas in the FEM second- or third-order equations are solved.

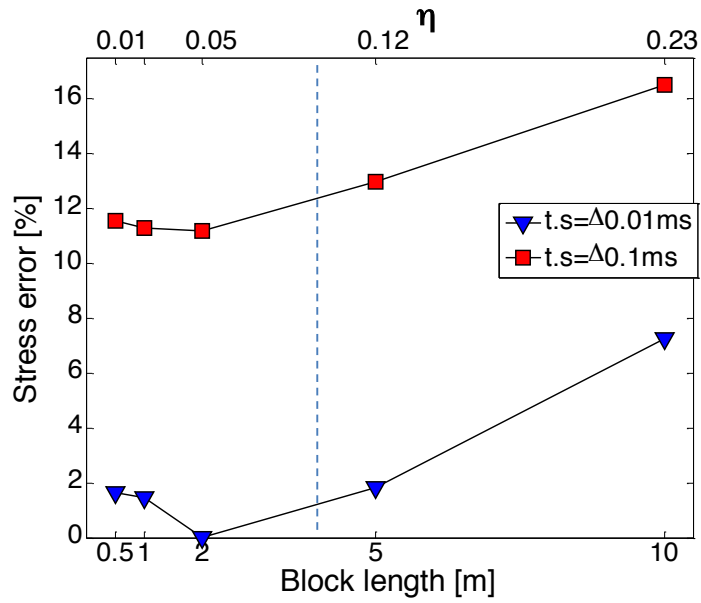


Figure 3.4- Comparison between the stress amplitude errors for two different time step sizes. The dashed line delineates $\eta=1/12$.

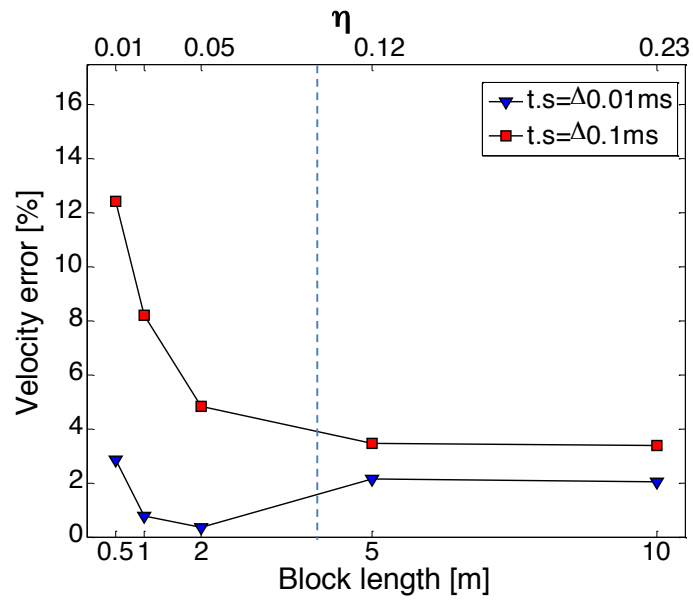


Figure 3.5- Velocity errors as a function of block (element) length for two time step sizes. The dashed line delineates $\eta=1/12$.

Chapter 4 - Blast shock simulation with DDA

Blasting is often used in surface and underground excavations, and usually sets off vibrations that propagate through the ground as displacement or stress waves. Those blast waves caused by the explosion gases occupy a much greater volume at ordinary confining pressures than the original charge and are capable of building up transient peak pressures of 105 atmospheres (atm) or more in the vicinity of the charge (US army engineers, 1972). Following the detonation, a shock wave generated within a few milliseconds (msec) propagates away from the explosive charge. Typically, even the strongest rocks will be shattered in the immediate vicinity of the blast source.

A typical blast loading pressure on an object can be characterized by its peak reflected pressure (P_0) and positive phase duration (t_0), as the negative phase is usually ignored (Figure 4.1.). This time history is very often simplified further into either a triangular or an exponential type loading in the available literature. The exponentially decaying loading function adopted here, can be expressed mathematically as:

$$P_{(t)} = P_0 \cdot e^{-\frac{(t-1.1t_a)}{t_a}} \quad t \geq 1.1t_a \quad (18)$$

Where P_t and P_0 are the shock stress at time t and the peak shock stress, respectively, t is time from blast, and t_a is the arrival time to distance R :

$$t_a = R/c \quad (19)$$

Where c is the characteristic material velocity.

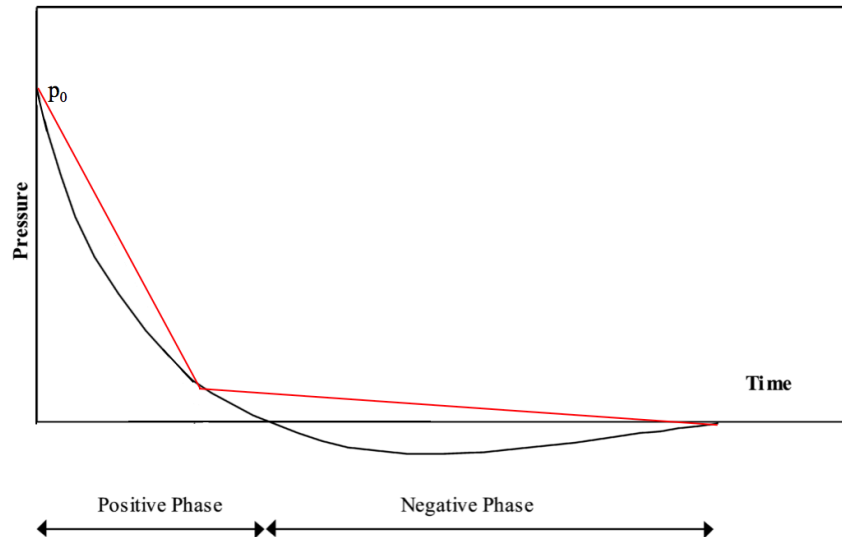


Figure 4.1- Explosive pressure time history. P_0 is the maximum pressure, the red line is the simplified function used as input for DDA modified after Low (2001).

4.1 Model geometry

The motivation for this simulation was to validate a blast model for DDA (see Figure 4.2). To simulate a radial propagating shock wave, eight blocks shaped as hollow octagons with 1m edges (Figure 4.3) were designed in order to transmit a shock wave to the rock mass.

The measurement points in the DDA model are aligned horizontally and vertically from the blast area. The peak force in this simulation is 10,000 kN. Upon reaching the edge of the DDA blast model, it will induce a radial stress of 10 MPa. Measurement points are placed horizontally and vertically from the blast area and are used to confirm that the simulated peak particle velocity (PPV) attenuation results are in agreement with the expected analytical solution.

The modeled domain boundaries (Figure 4.4) are set with the non-reflective boundaries to simulate an infinite medium. The discretization is carried out by dividing the rock mass into rectangular blocks, the area of which is refined horizontal and vertical to the blast. For this mesh the rock density, Young's modulus, and Poisson's ratio were 2563 kg/m³, 25 GPa, and 0.333, respectively. No-initial stresses are introduced for this validation simulation. The discontinuity friction angle is set to 45° everywhere in the

modeled domain. According to the results of the calibration study for P-wave propagation through an elastic bar presented above an optimal time step of 10^{-5} s was chosen.

In order to isolate the blast vibration from numerical background noise all simulations were tested both with and without a blast. Then, the non-blast simulation outputs were subtracted from the blast simulation outputs, thus filtering out all unnecessary background noise, and allowing us to detect arrivals that result only from blast wave propagation.

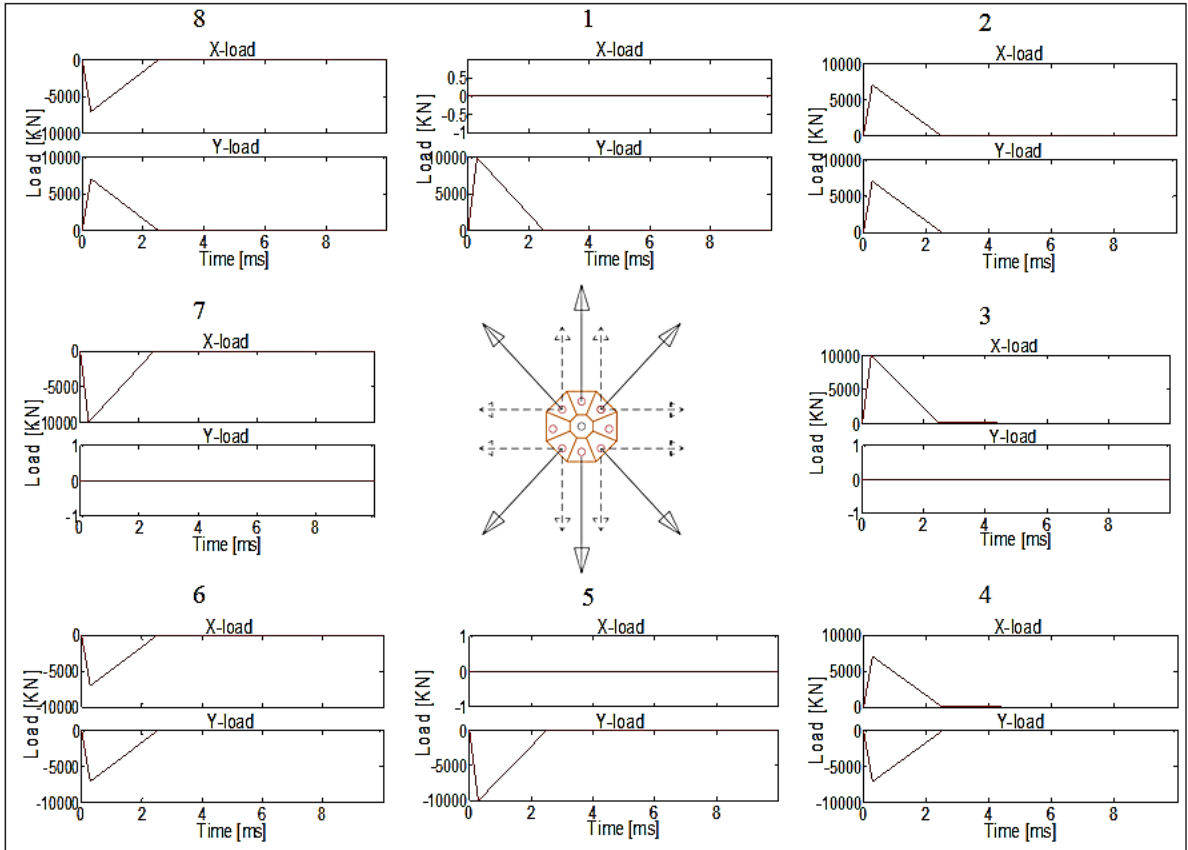


Figure 4.2- The blast load function used as input in every loading point around our DDA blast model

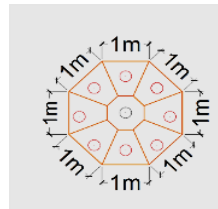


Figure 4.3- The DDA blast model used in this study.

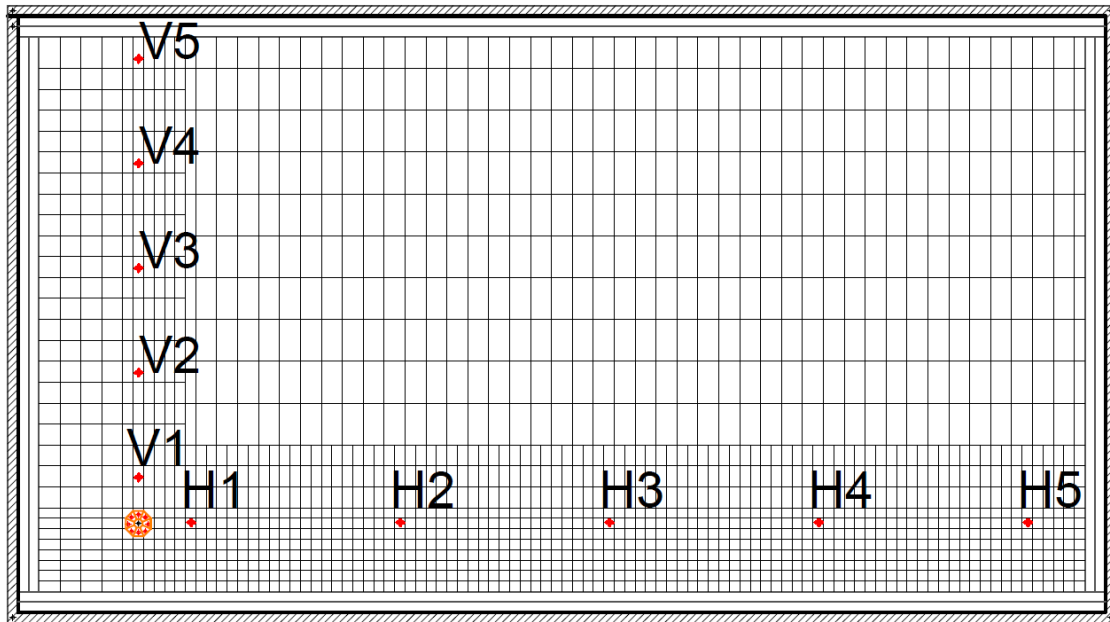


Figure 4.4- The configuration of the blast model, with a non-reflective boundaries at the boundaries of the modeled domain and position of measurement points in the horizontal (H) and vertical (V) directions.

4.2 Results

The filtered horizontal and vertical stresses as recorded at the measurement points from 0.1 sec before to 0.1 sec after the blast displays in Figure 4.5 and Figure 4.6. The stress in the closest measurement point is the largest, and decreases away from the blast. The largest stress measured in the horizontal direction is 5.14 MPa, whereas the largest stress measured in the vertical direction is 8.17 MPa. There were no reflected waves from the boundaries, confirming the efficiency of the implemented viscous boundary condition as developed by Bao et al. (2012). The first arrivals of the shock wave are clearly evident in both monitored directions.

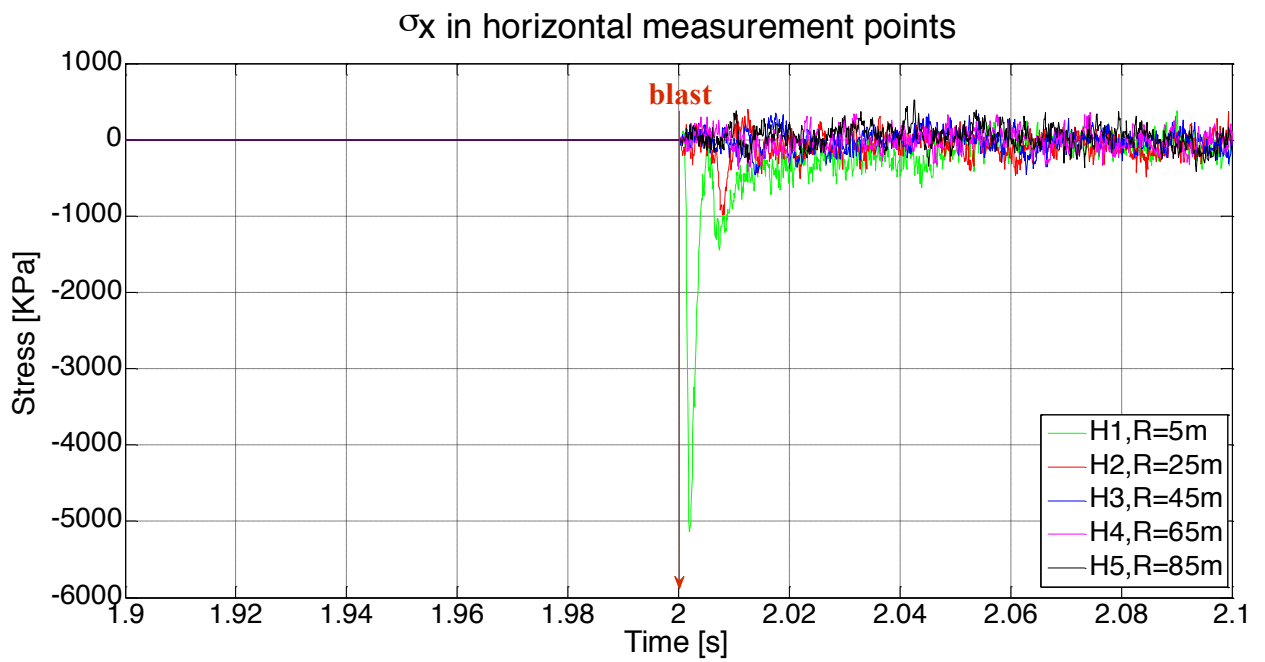


Figure 4.5 - Horizontal stress history +/- 0.1 s from blast.

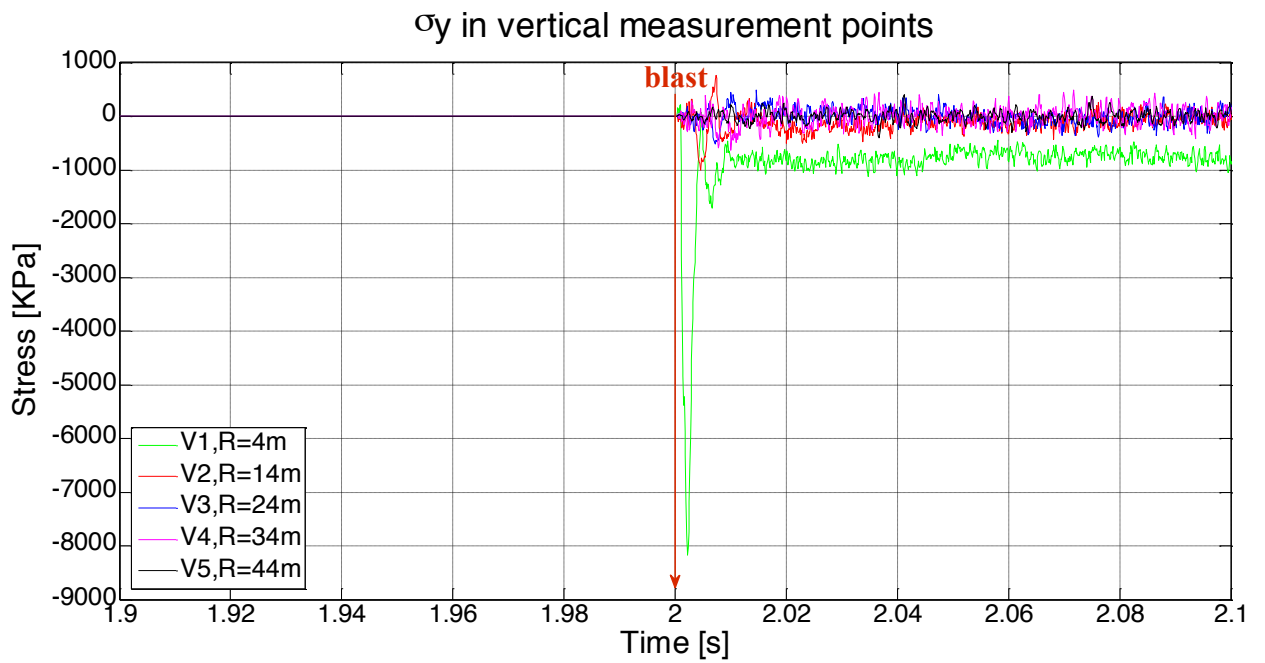


Figure 4.6 - Vertical stress history +/- 0.1 s from blast.

4.3 Discussion

The material velocities in the numerical DDA model are calculated from the arrival time of the peak velocity, and are compared with the theoretical value of the P-wave velocity for the material, as obtained from equation (11). Inspection of the numerically obtained peak stress and velocities reveals that P-wave arrival times are very close to the expected arrival times considering the characteristic material velocities (see Table 4.1), as would be obtained from equation 11. The numerical errors presented in Table 4.1 in the mid-range are acceptable, less than 15%; however, near the blast, the errors are unacceptably high. We attribute these unacceptable errors to the way the error is estimated, see equation (15), where values obtained at very small time intervals yield higher error results; a mathematical artifact.

Another source of error may be associated with the “algorithmic damping” (Doolin & Sitar ,2004) or “numerical damping” (Ohnishi & Nishiyama ,2005) inherent to the time integration scheme employed in the DDA method. A more careful inspection at the average error at the mid-range (measurement points #2–#4), shows a slightly greater accuracy in the vertical direction with an average error of 6.6% compared to the horizontal, where the average error is 7.4 %. This confirms our previously obtained results concerning the optimal block length in the modeled domain with respect to wave length of the incident wave. In the horizontal direction, the block length is 1m, whereas in the vertical direction, it was 2m. Namely the block length in the horizontal direction is too small, resulting in increased errors (see Figure 3.4 and Figure 3.5).

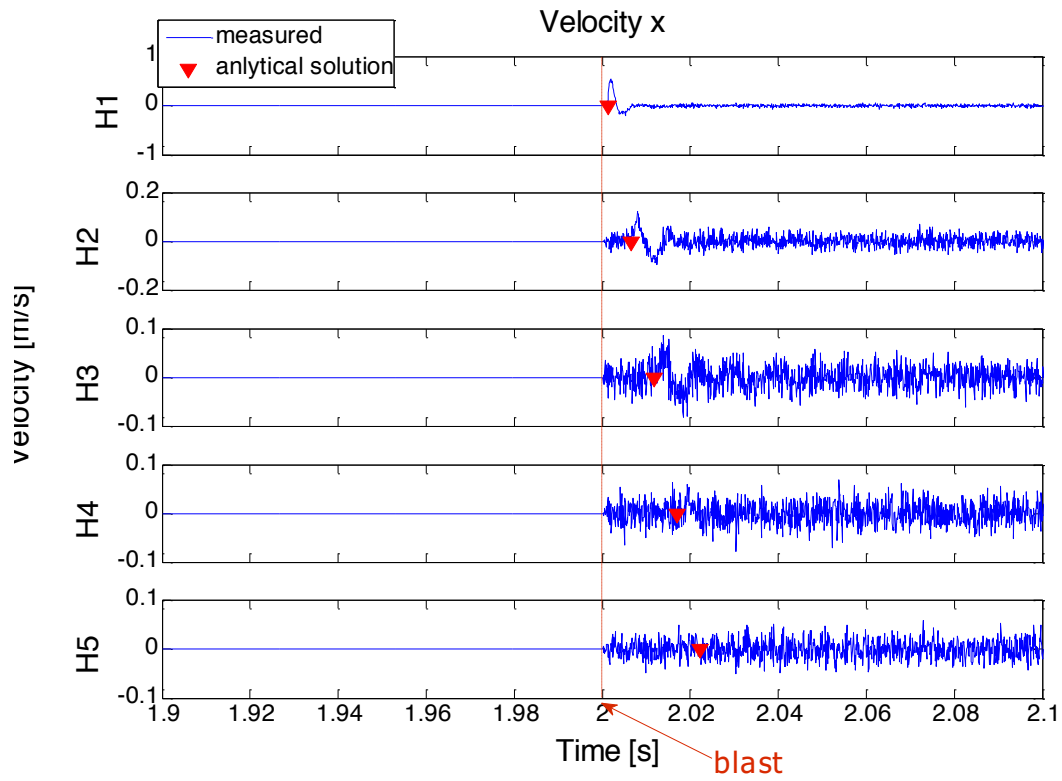


Figure 4.7 - Velocity time history in the horizontal direction. The blast accrued at 2 seconds.

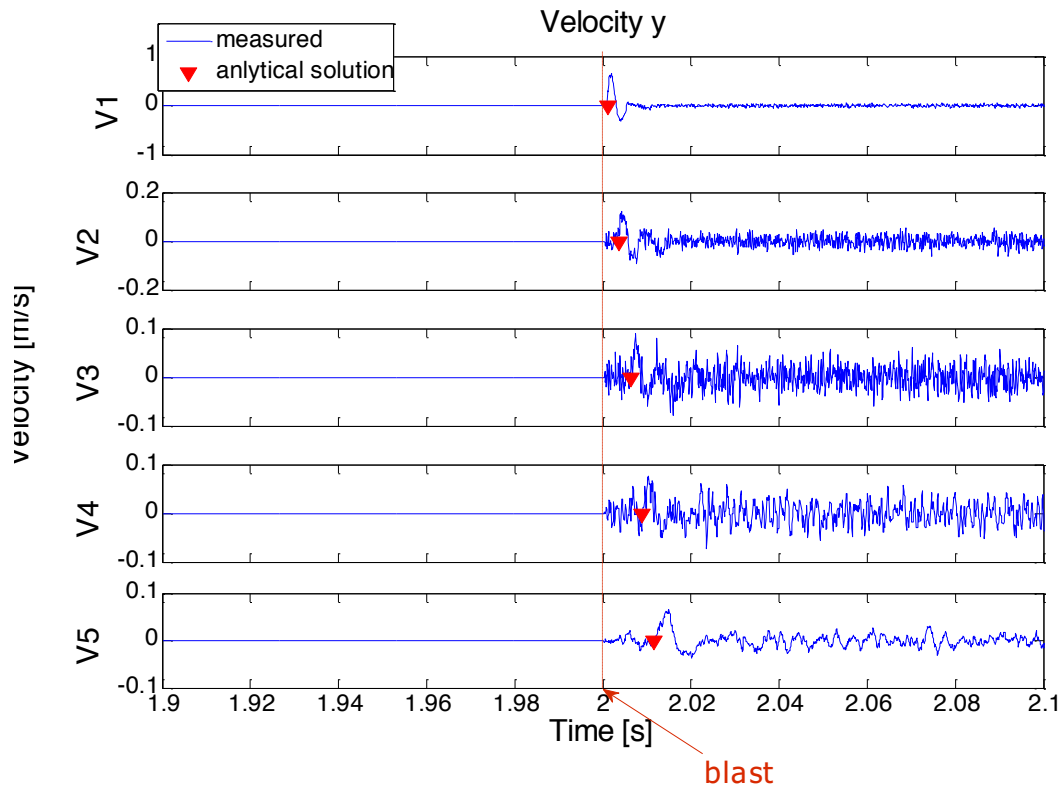


Figure 4.8 - Velocity time history in the vertical direction. The blast occurred at 2 seconds.

Table 4.1: Peak arrival time errors in the different measurement points.

Measurement point	H1	H2	H3	H4	H5	V1	V2	V3	V4	V5
Actual time of peak [ms]	1.96	7.96	13.96	19.36	N/A	1.96	4.26	7.46	10.36	14.96
Predicted peak time [ms]	1.43	7.18	12.94	18.69	24.44	1.15	4.02	6.9	9.778	12.65
Error [%]	36.23	10.70	7.87	3.57	N/A	70.29	5.78	8.07	5.95	18.22

Chapter 5 - Validating shock-wave modeling with DDA using the Jinping case study

5.1 Jinping II Hydropower Station as a case study

The Jinping II Hydropower Project is located at the Great Jinping River Bend of the Yalong River in the Sichuan province of China, see Figure 5.1a. It is one of the greatest tunneling projects in the world in which the water is diverted by a sluice needle dam from the river to headrace tunnels to be used for generating power. There are seven parallel high pressure tunnels in total: four diversion tunnels, two auxiliary tunnels, and a drainage tunnel (Figure 5.1c). The four diversion tunnels have a diameter of 12–13m and a total length of 16.67 km, and are constructed mostly at a depth of 1500–2000 m, where in some places the maximum overburden is up to 2525m. The tunnels are mostly excavated in marble (Shiyong et al. 2010). Considering these parameters, the project faced a series of difficulties, such as high geostress (max = 70 MPa), rockburst, and instability of the surrounding rock mass.

As a result of frequent events of rockbursts that occurred during the excavation of the tunnels, this project provides a case for many studies on rockbursts (Feng et al. ,2013; Li et al. ,2012; Shiyong et al. ,2010; Zhang et al. ,2012). As part of the research and in order to reduce the rockbursts risk for construction safety, a high-performance integrated seismic system was adopted in the tunnels for rockbursts monitoring and warning. Here, we collaborate with Feng et al., (2015) from the Chinese Academy of Sciences. We use their analysis to validate the shock-wave modeling in this current study. Feng et al., (2015) utilized a three-dimensional micro-seismic (MS) monitoring system that was placed at the worksites. This technique allowed them to calculate the source location of the rockburst through sectional velocity modeling. Here, we applied Feng et al., (2015)'s source location and calculated velocity in our simulations.

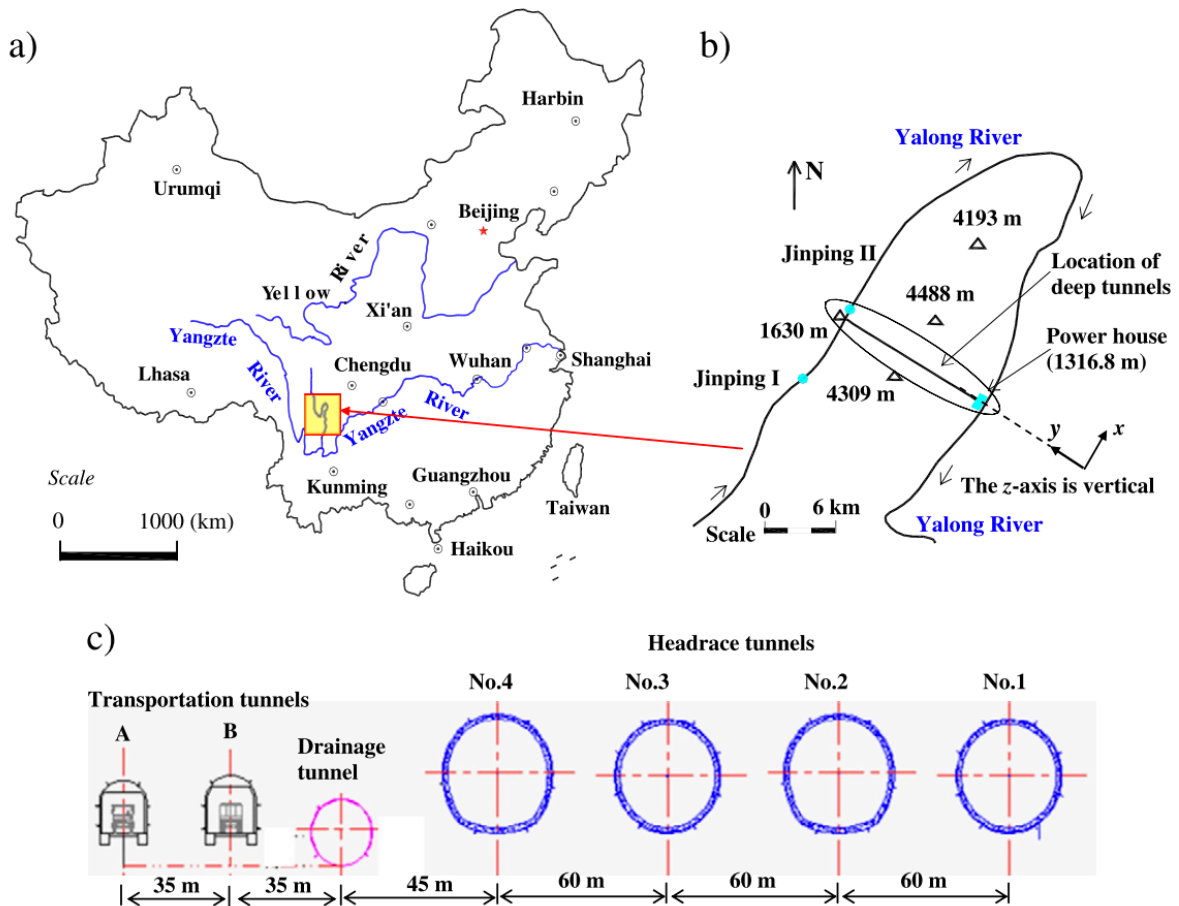


Figure 5.1 Location and plan of the Jinping II Hydropower Station: (a) Location of the Jinping project in China, (b) Layout of the Jinping Hydropower project across the Yalong River, (c) Configuration of seven tunnels (Li et al. ,2012)

5.2 Model geometry for validation study

The rockburst simulated for this validation occurred in headrace tunnel #3 on 9 September 2010 around 20:32. Information about the rockburst, MS sensor locations, and P-wave triggered times from Feng et al., (2015) is shown in Table 5.1

The layout of the in-situ monitoring campaign is shown in Figure 5.2. Due to the limited space, personnel, and safety equipment available, MS sensors were laid out behind the working face in distributed groups (Feng et al. ,2013; Chen et al. ,2013). MS sensors close to each other in the axial direction along the tunnel are regarded as a group (Feng et al. ,2015).

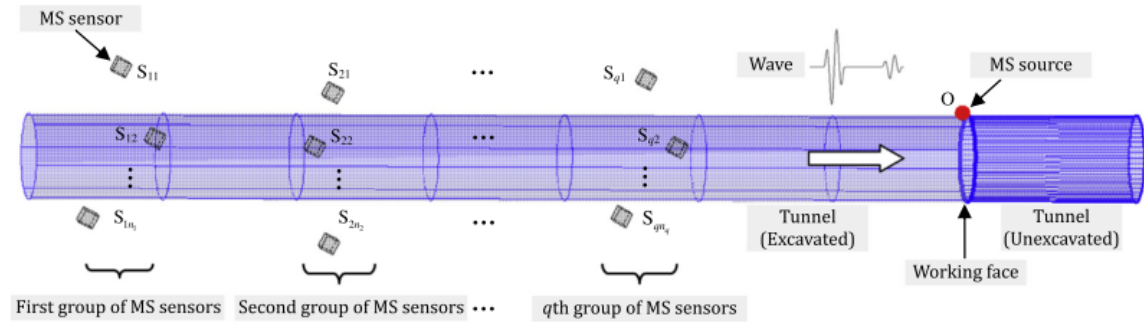


Figure 5.2 - Diagram showing MS monitoring in the tunnel (Feng et al. ,2015)

Table 5.1: Coordinates of sensor in the tunnel

MS site name	Coordinates (m)			Distance from rockburst (m)	Triggered time of P wave
	X	Y	Z		
S1-2	10245.5	1	-30.5	108	20:32:33.287857
S1-4	10247.2	7.2	-39.8	107	20:32:33.288190
S2-1	10215.7	0.7	-30.6	81	20:32:33.283023
S2-4	10219.3	-6.4	-39.3	77	20:32:33.283858

The 2D-DDA model of the tunnel is 120m long, with the two groups of MS sensors simulated using measurement points placed in the model according to the reported MS sensor location sites in tunnel #3 (measure point S1-2, S1-4, S2-1 and S2-4, as shown in Figure 5.3). In addition, two measurement points were placed in the edges of the modeled domain for control prepresses (measurement points 5 and 6 as shown in Figure 5.3). Our DDA blast model is used to simulate the focus of the rockburst detected in the field.

The blocks length and height in the DDA model around the tunnel where greater resolution is sought are 1m and everywhere else, the block size is increased to 2X2m blocks to obtain a more efficient use of available CPU power.

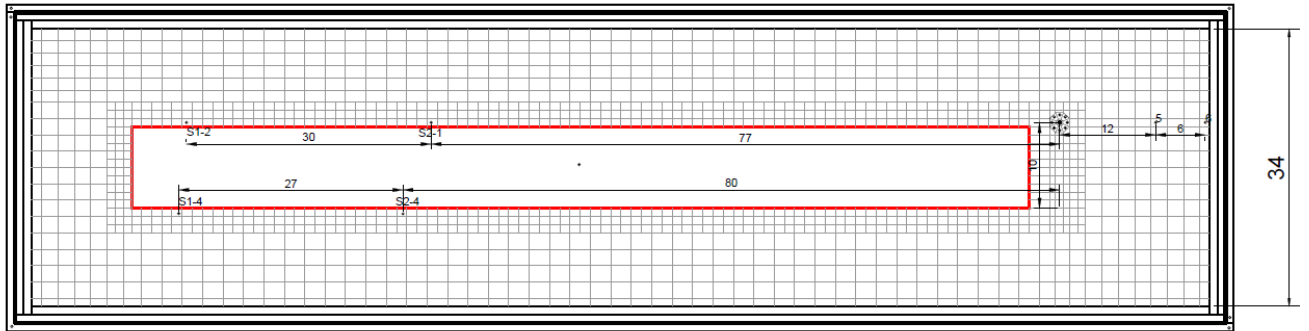


Figure 5.3 – The DDA model of the monitored tunnel segment at Jinping with location of measurement points used for validation.

The Jinping tunnel was mostly excavated in marble, the characteristic parameters of which are listed in Table 5.2 following data published by Li et al. (2012). To prevent the ceiling from collapsing in the DDA model once the simulation begins due to gravitational pull as no support is inserted in the model or in the field, the simulations are performed under zero gravity, while the elements retain their density of course, so that the weight of all blocks in the modeled domain is zero.

Table 5.2: Rock properties at the studied section of the Jinping Hydropower project (tunnel F) following results published by Li et al. (2012).

Rock type	Marble
Young's modulus (GPa)	25.3
Poisson's ratio	0.22
Tensile strength (MPa)	1.5
Initial cohesion (MPa)	23.9
Residual cohesion (MPa)	3.1
Residual internal friction angle (°)	46

The Mohr–Coulomb failure criterion is applied to model shear sliding along pre-existing discontinuities in DDA, and a discontinuity friction angle of 46° is assumed here for all discontinuities. Viscous boundaries as reviewed above are employed in the DDA simulations at the boundaries of the modeled domain to avoid artificial reflections from the boundaries that may obscure the results of the simulation. The time step size is set at 10^{-5} sec which, based on our prior result (Chapter 3 -), should minimize numeric errors in the given configuration.

5.3 Result

The results of the validation study of shock-wave propagation through a jointed rock mass are shown in Figure 5.4 and Figure 5.5. The principal stress trajectories at the end of the simulation are shown in Figure 5.4, suggesting that the rock energy returned to the original state after the blast. This and the velocity history of measurement points R1 and R2 (Figure 5.5) demonstrates very clearly the efficiency of the viscous boundary used as no reflections are measured in DDA at all. The DDA time histories for monitoring stations S2-1 and S1-2 (Figure 5.5) are in a very good agreement with the theoretical arrival times at each station. The actual arrival times, as measured in the field in each station, are plotted as (*), and they are clearly much earlier than those obtained either numerically or theoretically.

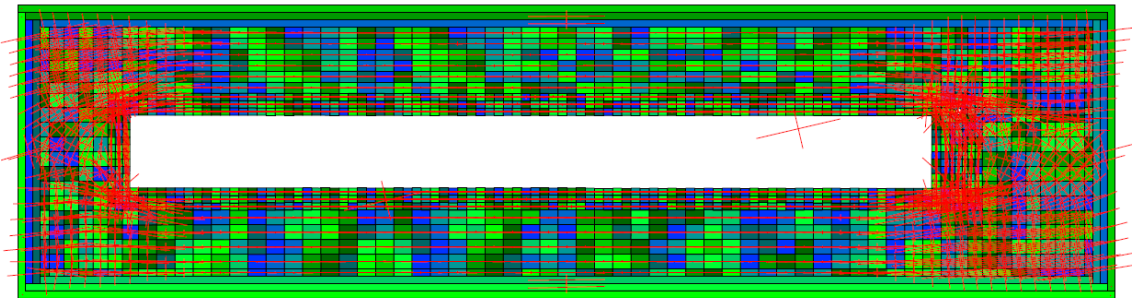


Figure 5.4- Principal stress trajectories in the modeled domain at the end of the simulation.

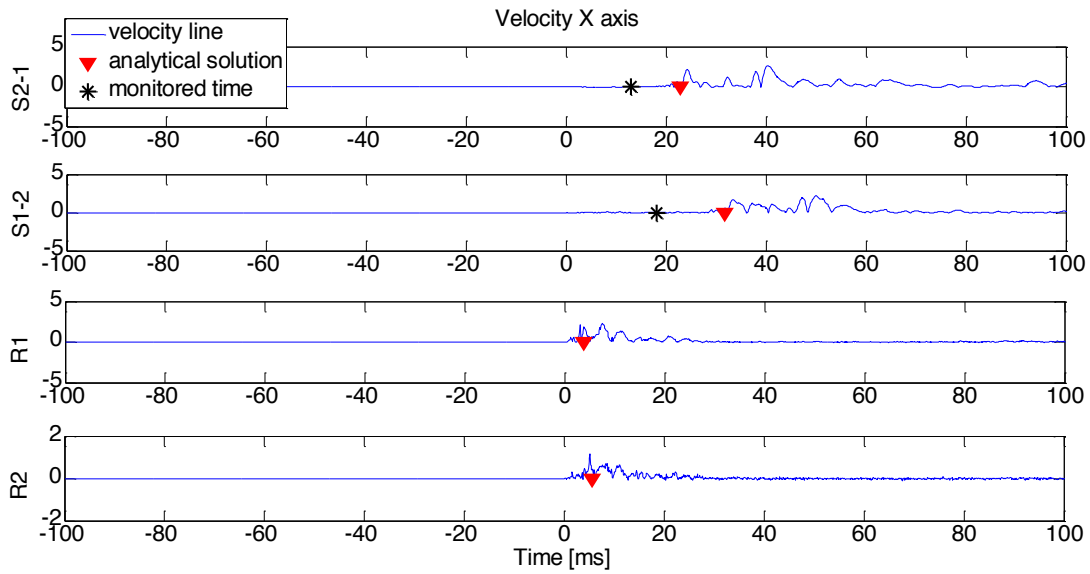


Figure 5.5- Velocity time history in the horizontal direction (blue line), theoretical arrival times of shock wave (red triangles), and arrival time in monitored points in the field (*).

5.4 Discussion

We believe the discrepancy between the numerical results, the analytical results, and the monitored time is due to differences in material properties between the assumed values for numerical or theoretical computations and the actually encountered ones in the field near the face. It should be pointed out that the rock mass parameters were not measured in the field exactly where the monitoring campaign was performed, but on samples taken from a nearby location (Tunnel F) (Li et al. ,2012), whereas the rockbursts and monitoring campaign was performed in Tunnel #3, 140m away. Still the resemblance between the numerical results and the analytical results is satisfying enough to validate the use of the DDA for rockburst simulations.

Chapter 6 - Strain Rockbursts Simulations with DDA

Here we explore rockburst initiation due to strain relaxation in an initially discontinuous rock mass. In concept, this mechanism is manifested as the ejection of a portion of the tunnel-wall (or floor or roof) directionally associated with a transient shock wave. Freedom of movement, and sometimes the shape of the ejected blocks of rock, are usually dictated by the presence of existing jointing or induced fracturing (Ortlepp & Stacey ,1998). Block theory (Goodman & Shi ,1985) provides a robust and elegant method to detect the removable key blocks in the rock mass, their failure mode, and limiting equilibrium under both static and pseudo-static conditions. A schematic illustration of strain relaxation mechanism is shown in Figure 6.1.



Figure 6.1 Ejection-type rockburst results from expulsion of joint or fracture-defined block of rock. (Ortlepp & Stacey ,1994)

Once the excavation is created, stress redistribution will take place where tangential stresses (i.e., major principal stress σ_1) increase while radial stresses (the minimum principal stress σ_3) decrease to zero around the opening, resulting in the development of maximum shear stresses, i.e., $\tau = (\sigma_1 - \sigma_3)/2$, at the newly created opening boundary. Where and when the maximum shear stress exceeds the frictional resistance of pre-existing joints, instantaneous sliding will occur provided the blocks are finite and removable, consequently emitting strong seismic vibrations, which will propagate through the discontinuous rock mass. Such an event may be considered as a rockburst generated by slip of removable blocks along pre-existing discontinuities. Since the shear

strength of pre-existing discontinuities is much lower than that of intact rock elements, it is much more likely that, at critical locations around the tunnel boundary, the increased shear stress will exceed the level of available discontinuity shear strength before it approaches the level of shear strength of intact rock elements. Therefore, rockbursts due to dynamic ejection of key blocks in the process of strain relaxation are much more likely in relatively strong, discontinuous rock masses than due to fracturing of intact rock elements.

Instability due fault slip results from the constitutive behavior of the rock material, and may involve shearing, splitting or crushing of the intact rock (Brady & Brown ,2007). In addition to unstable material rupture, tunnel instability and seismicity may arise from unstable slip on planes of weakness such as faults or other discontinuities of the rock mass in the tunnel surrounding. For example, Rorke & Roering (1984) report first motion studies which suggest a source mechanism involving shear motion. Spottiswoode (1984) has proposed that unstable fault slip plays an significant role as the source of rockbursts, supported by interpretation of field observations of rock mass deformation attending rockbursts reported by Ortlepp (1978). Gay & Ortlepp (1979) verified this observations and described in detail the character faults induced by mining that exhibited clear indications of recent shear displacement.

The mechanics of unstable slip on a plane of weakness such as a fault has been considered by Rice (1983). His model of rock mass instability requires that the potential slip surface exhibit peak-residual behavior. Therefore, in rock mass instability analysis, joint deformation involving displacement weakening must be taken into account (Brady & Brown ,2007). However, for faults, which are at a residual state of shear strength, the displacement-weakening model cannot be justified, and alternative concepts of unstable deformation must be considered.

The mechanism of energy redistribution has the same manifestation as in the case of strain bursts but here the source of the energy is different. The source of energy that leads to this type of rockbursts is a seismic event or blasting related to the excavation itself, the focus of which may be at some distance from the damage zone. Therefore, in this mechanism the source and damage locations are not coincident. The extent and violence

of the damage that occurs depends on the amount of energy and the proximity of the source from the tunnel (Ortlepp & Stacey, 1994).

The influence of the excavation process on the surrounding rocks is particularly severe during blasting (Yan et al., 2015). Studies on the relation between blasting and rockbursts have been reported since the 1950s (Leet, 1951). With the development of tunneling methods, which increase both the excavation footage and the charge weights in blasting techniques, the contribution of excavation disturbance to the generation of rockbursts is even more significant. Nevertheless, the blasting disturbance is neither a sufficient, nor a necessary requirement for rockbursts. Xie & Li (2004) and Xu et al. (2003) studied the influence of repeated blasting disturbances on the inoculation of rockbursts, and confirmed that blasting disturbances could be regarded as a significant controlling factor for rockbursts in addition to acting as an important exciting or triggering factor. Wang and Huang (1998) also found that a blasting induced disturbance can seriously affect the scale of rockbursts. Therefore, research on effects of blast-induced shock waves to underground tunnel damage is both significant and practical (Zhao et al., 1999).

We argue in this thesis that before rockbursts will be induced by fracture propagation through intact rock elements in the rock mass, existing removable key blocks, formed by the intersection of pre-existing discontinuities in the rock mass, will be ejected from the rock mass into the excavation space, because of the much lower shear strength of the discontinuities. We use here, therefore, a discrete element numerical approach. We chose to use the numerical, implicit, discrete element DDA method (Shi, 1993), because it has been thoroughly validated and verified for rock engineering problems involving dynamic analysis, both by BGU researchers as well as many research groups worldwide.

6.1 Strain relaxation mechanism for rockburst generation

6.1.1 Model assumptions

The analyzed cross section is shown in Figure 6.2 where the diameter of the circular tunnel is 10 m, and the joints are inclined at 60° to the horizontal. The input friction angle for all discontinuities is 65° degrees. Non-reflective boundaries are added at the boundaries of the jointed domain to simulate an infinite domain. To allow for “gravity turn on” (MacLaughlin & Sitar ,1999) the modeled domain was subjected to gravitational loading with no tunnel for 2.5 sec under the imposed initial in-situ stresses to allow “setting” of the contact springs and for the imposed stresses to attain their pre-specified level everywhere in the modeled domain (Tal et al. ,2014). To restrain artificial numerical vibrations, we applied 1% kinetic damping to the simulations. The contact spring stiffness (g_0) was set to ten times the Young’s modulus: 2.5×10^{-11} N/m. No cohesion and tensile strength are assigned to the joints, the rest of the input parameters are listed in Table 6.1

Measurement points 1, 2, and 4 were placed in the key blocks that were identified according to the block theory (Goodman & Shi ,1985). Measurement point 3 was placed in the right sidewall of the tunnel to monitor the stress evolution. Measurement point 5 was placed 20m away from the tunnel for control.

Table 6.1: Rock mesh properties:

Density (kg/m^3)	2563
Young’s modulus (GPa)	25
Poisson ratio	0.333
Discontinuity friction angle ($^\circ$)	65
σ_x (MPa)	[0 10 30 50]
σ_y (MPa)	[0 10 30 50]
τ_{xy} (MPa)	0

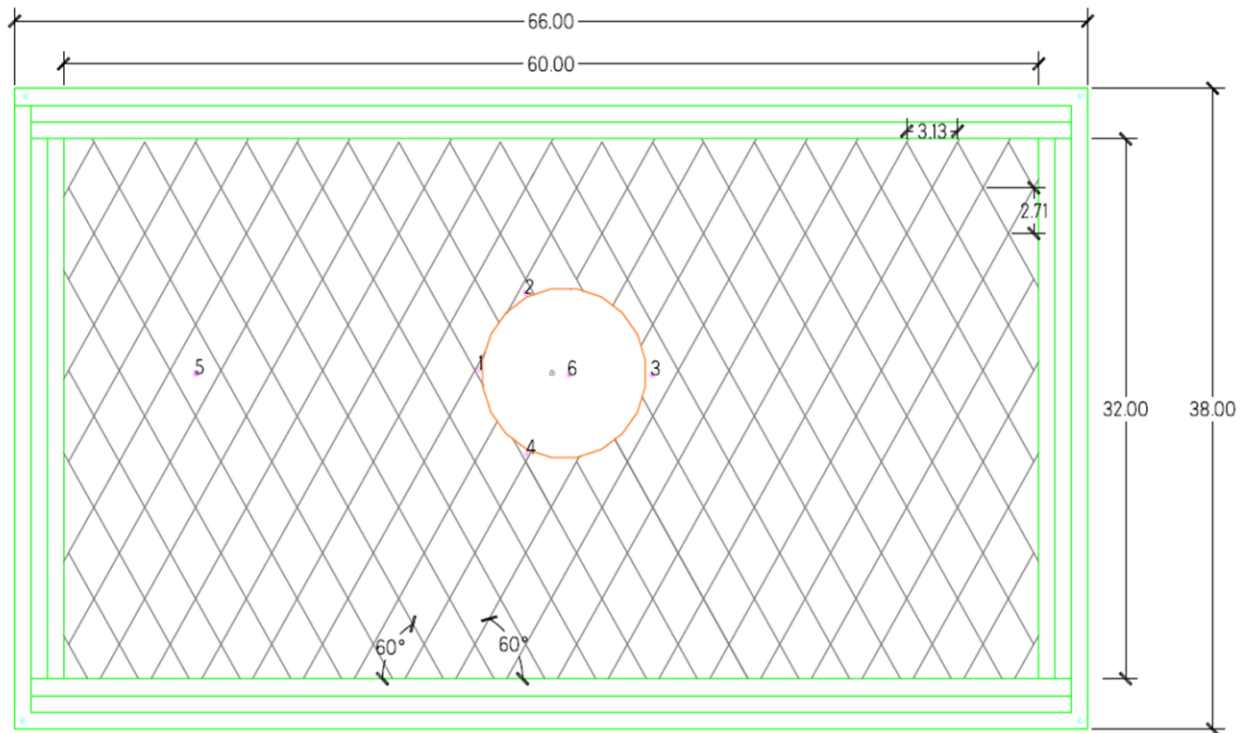


Figure 6.2- DDA mesh of analyzed domain coupled with AutoCAD preprocessing.

6.1.2 Simulation result

We begin by exploring the role of the initial in-situ stresses. Four simulations are performed under initial hydrostatic stresses of [0 10 30 50] MPa. The analysis will focus on Key Block No. 1 (Figure 6.2). Under static loading this block will be stable, as the assigned friction angle of the joints is greater than the inclination of the sliding plane. This was confirmed with DDA when tunnel was removed in a simulation with zero initial in-situ stress.

Vertical and horizontal stress histories in blocks with measurement points 3 and 5 (see Figure 6.2) are plotted in Figure 6.3 a and b, respectively, for the four different levels of imposed initial hydrostatic stress conditions. It can be seen that in all the simulations a response to strain relaxation was recorded in both points. However, measurement point number 3, on the tunnel wall, displays a more powerful reaction to strain relaxation compared to the reaction in point 5 regardless of the level of initial stress, as would be

expected. With increasing level of initial in-situ stress the response is the measurement is distinctly stronger.

Measurement point #1 (block 1) was placed in the left sidewall of the tunnel and measurement point #2 (block 2) was placed in the roof of the tunnel. When observing the result (Figure 6.4) we find out that block 2 was mostly stable in all simulations with initial stress and failed in falling mode only in the simulation with no initial stress.

The displacement evolution of block 1 is shown in Figure 6.4 for different levels of initial stresses as well as the graphical output of the block system as computed with DDA.

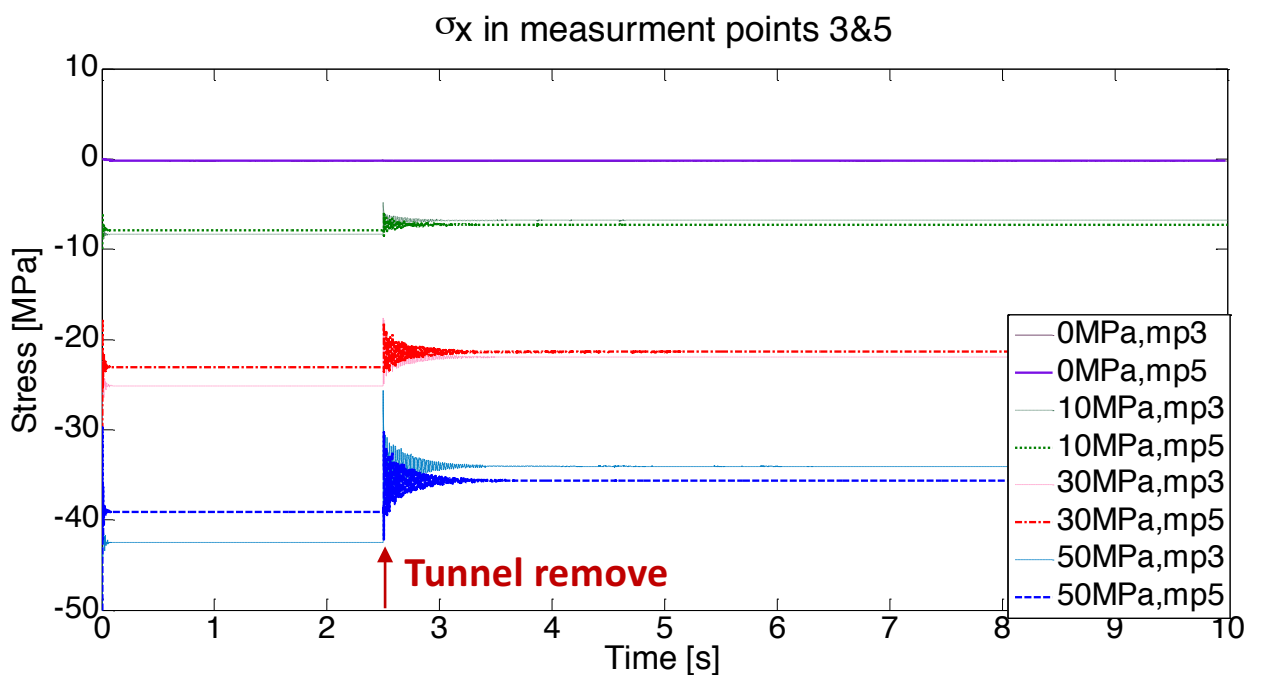


Figure 6.3- Axial stress in measurement point (mp) 3 and 5

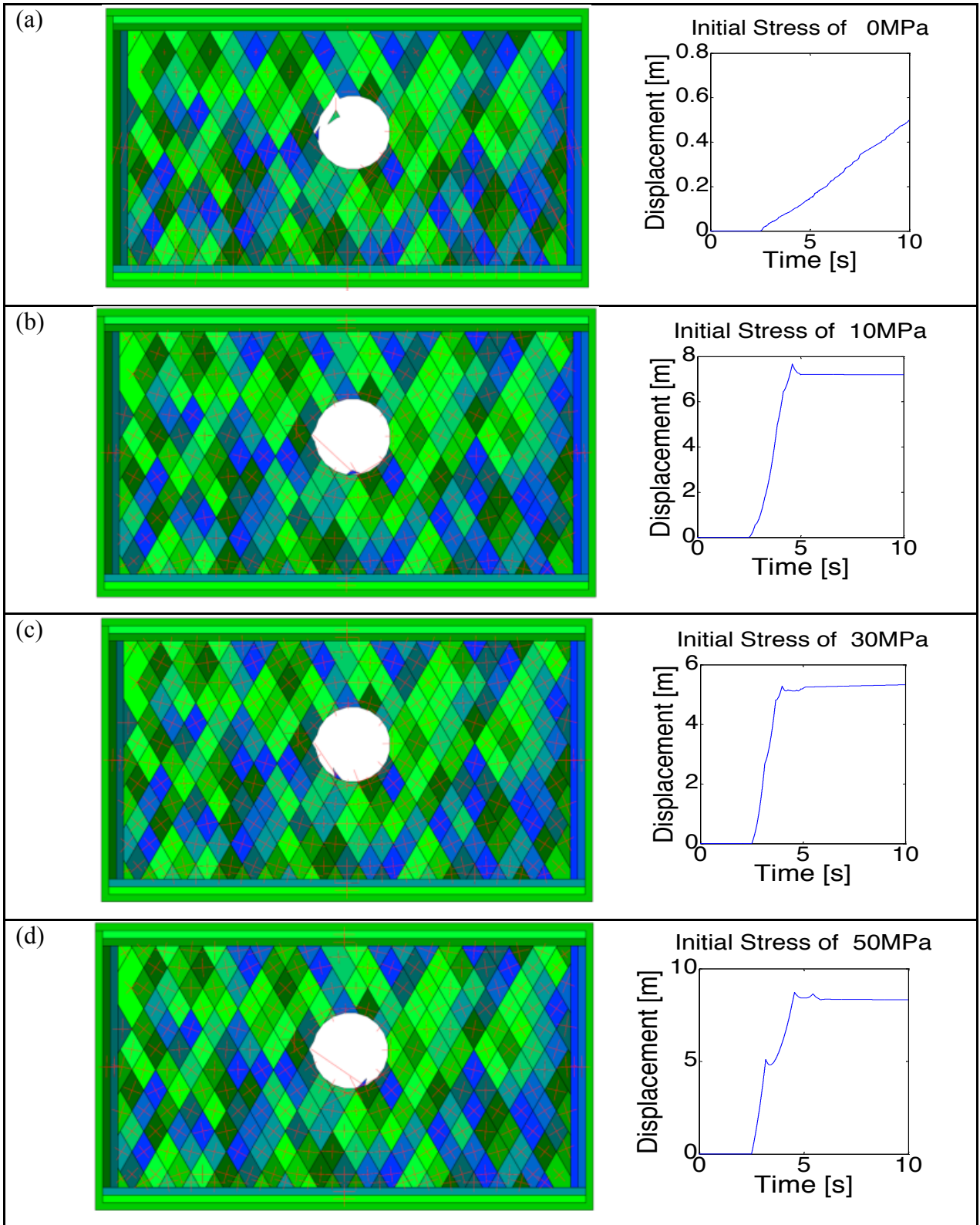


Figure 6.4- The result of the strain-relaxation simulations for initial stresses of (a) 0 MPa ,(b) 10 MPa, (c) 30 MPa, (d) 50 MPa.

6.1.3 The role of initial stresses

The rockbursts discussed in this experiment fall into the category of “fault-slip” type discussed in the introduction, where the discontinuities already exist, and the intersections of which form key blocks that are likely to fail provided that sufficient energy is supplied by the strain relaxation mechanism.

Examination of the response of key block 1 to strain relaxation (Figure 6.5) clearly shows that with increasing level of initial stress the displacement, velocity and acceleration of the ejected block increase.

The Code for Geological Investigations of Hydropower Engineering’s (CGIHE), proposed by the National Standards Compilation Group of China (2008) (In Chen et al., 2013), suggests that when there was an initial load on the tunnel surrounding all the rockbursts that occurred could be classified as extremely intense based on the depth and extent of the failure. Whereas rockbursts documented in low or zero initial stress conditions were classified as weak rockburst. It may be concluded, both from the numerical results presented here and empirical results compiled by others, that the initial loading has a significant influence on the intensity of the rockbursts, where an initial stress level of 10 MPa seems to be a lower threshold, corresponding to an overburden of some 400m.

The relationship between the ejected key block peak velocity and acceleration as a function of the initial stress level is plotted in Figure 6.5 where a linear trend may be depicted. It may be concluded, therefore, that in a tunnel subjected to high initial stresses, once the tunnel space is formed existing key blocks in the rock mass which are stable against sliding under static conditions may be ejected into the space, provided the initial stresses that are relaxed are sufficiently high.

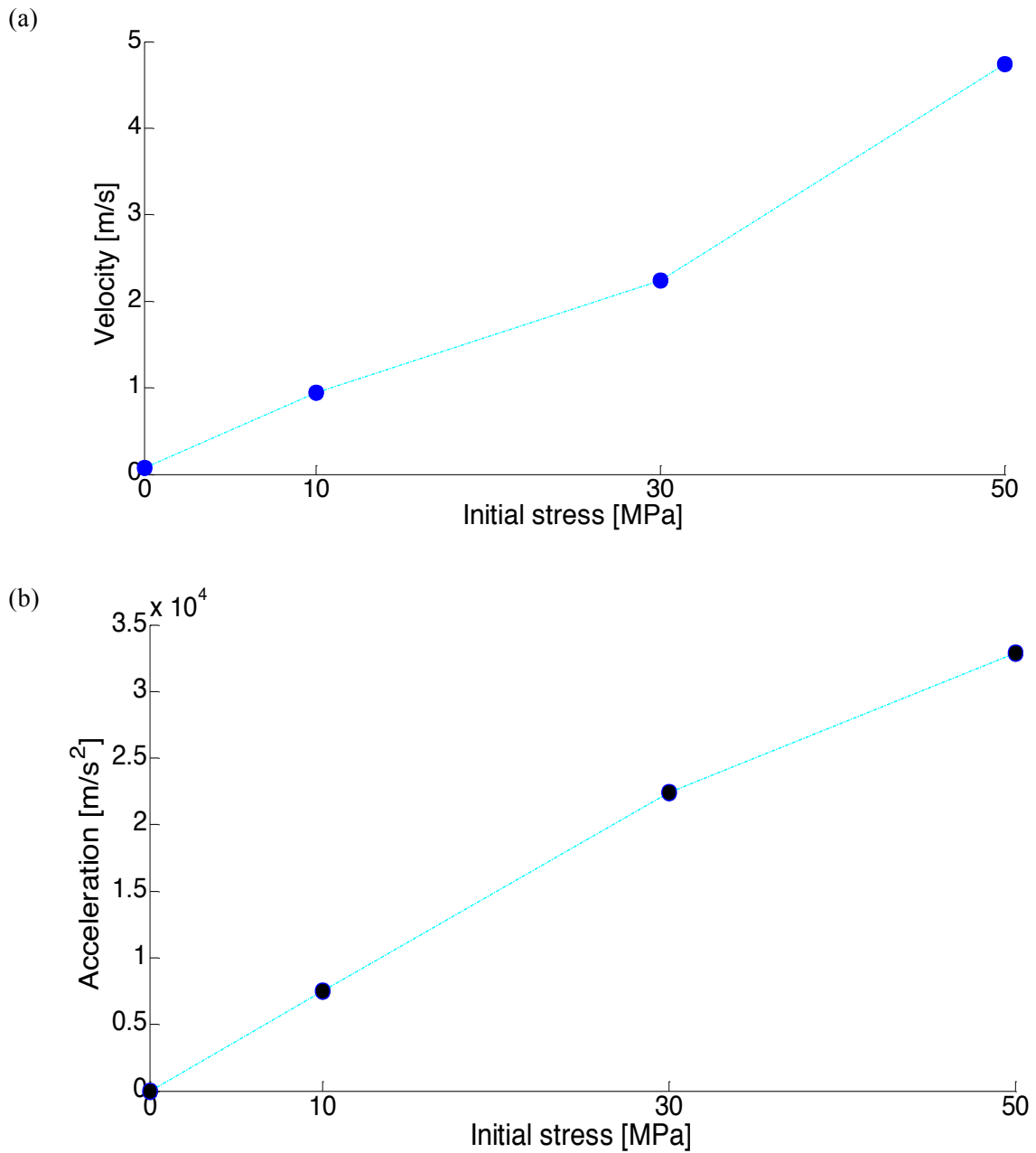


Figure 6.5- The relation between the initial stress of the rock mass and the velocity (a) and acceleration (b) of the ejected key block (no. 1) in response to the excavation induced strain relaxation.

6.2 Energy redistribution mechanism for rockburst generation

6.2.1 Model assumptions

The rock mass structure was generated in a way that ensures block stability in the sidewalls (see Figure 6.6) with block collapse restricted to the roof under static conditions.

Six measurement points are used in the mesh, four around the tunnel, where #1 is the closest to the blast element, #4 is in a removable block in the floor, #2 represents the ceiling right above block #4, and #3 is on the opposite sidewall from the blast. Measurement points 5 and 6 are the control points, # 5 between the blast and the tunnel, and #6 between the blast and the boundary of the mesh (see Figure 6.7).

The input rock properties for DDA are listed in Table 6.2. Discontinuity friction angles varied in the simulations from 0° to 45° under two initial hydro-static stresses: 0 and 50 MPa. The blast element is the same as the one presented in Chapter 4 -, and in this simulation, the maximum blast load is 60,000 kN. As before, in order to filter the blast vibration from numerical background noise, the simulation was performed twice with and without the blast, and the results without the blast were subtracted from the results with the blast.

Table 6.2: Input parameters for DDA.

Density (kg/m³)	2500
Young's modulus (GPa)	25
Poisson ratio	0.333
Discontinuity friction angle (°)	$\begin{bmatrix} 0 \\ 5 \\ 25 \\ 35 \\ 45 \end{bmatrix}$
σ_x (MPa)	[0 50]
σ_y (MPa)	[0 50]
τ_{xy} (MPa)	0

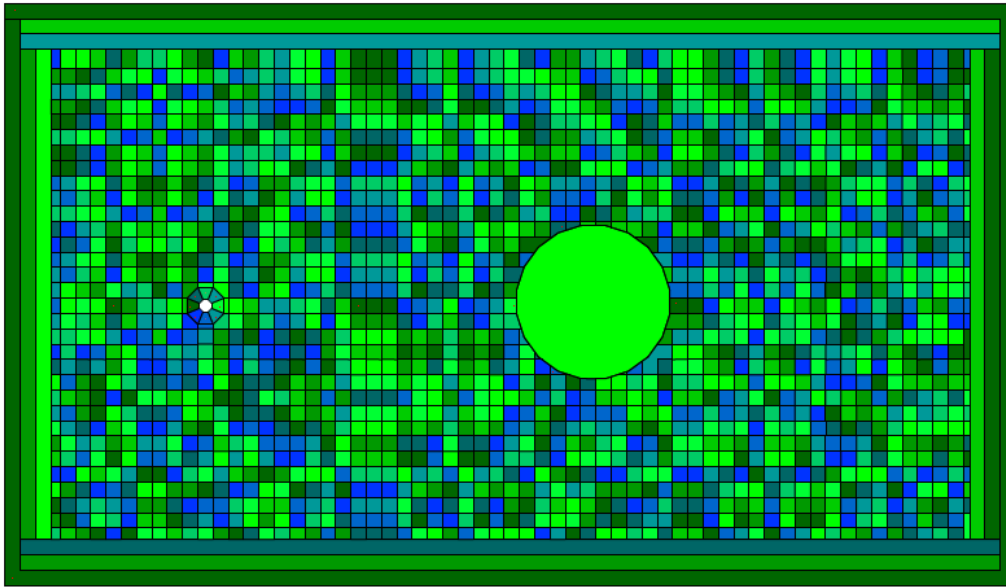


Figure 6.6- The simulated DDA model

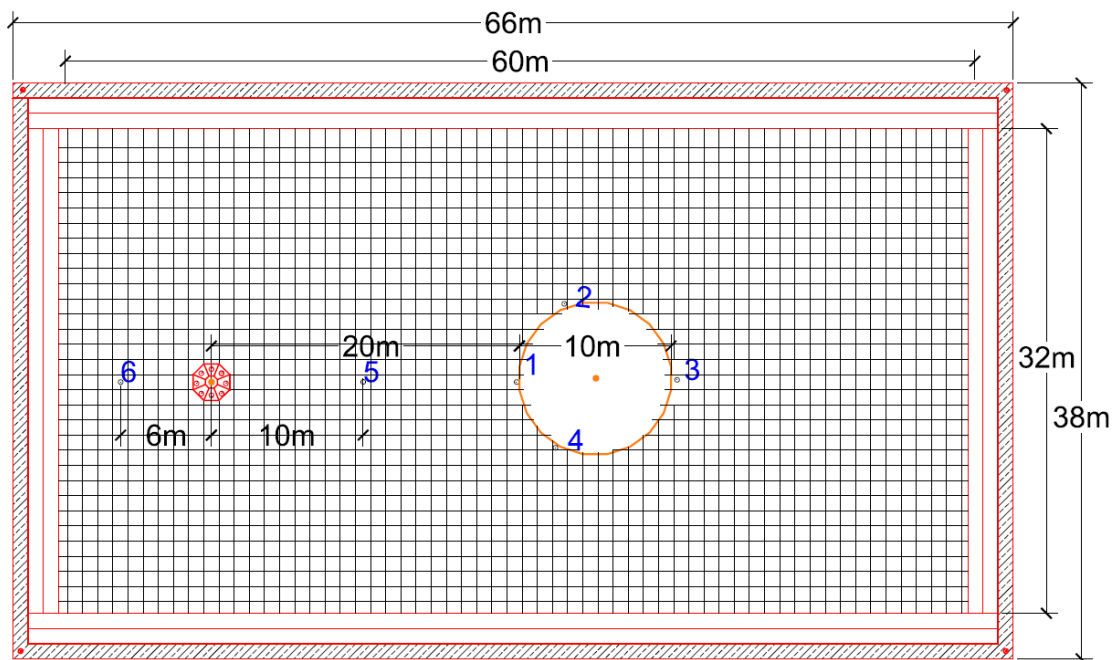


Figure 6.7- Model layout with dimensions and measurement point locations

6.2.2 Simulations results

The deformed mesh at the end of the simulations along with principal stress trajectories are shown in Figure 6.8 and Figure 6.9 with and without initial in-situ stresses for different values of joint friction angles. Inspection of the graphical output reveals that the entire tunnel collapsed only with zero joint friction; otherwise, it has attained a state of equilibrium after some initial block arrangement. Interestingly, block pop-outs from the floor can also be observed in several simulations.

To probe deeper into the tunnel response to the blast comparisons of stresses for the different discontinuity friction angles, with and without initial stresses, are presented in Figure 6.10 a and b. The response in measurement points 5 & 6 representing shock wave propagation through discontinuous rock is shown in Figure 6.10. Inspection of this response reveals that when the shock wave propagates under no initial confining stresses, the response of the rock mass, as measured in terms of the induced stresses in measurement points 5 and 6, is higher, with all stresses being compressive. As would be expected, the response measured in measurement point 6 is much higher than in point 5 because of its closer proximity to the blast.

From a physical point of view, the most natural manifestation of shock-wave propagation through the rock mass is the displacement that occurs as the vibration passes a given location. This particle displacement can be differentiated to obtain the particle velocity. Typically, it is the particle velocity or the particle acceleration of the blast vibration that are measured in practice in the field. The peak particle velocity and acceleration in the measurement points around the tunnel are shown in Figure 6.11.

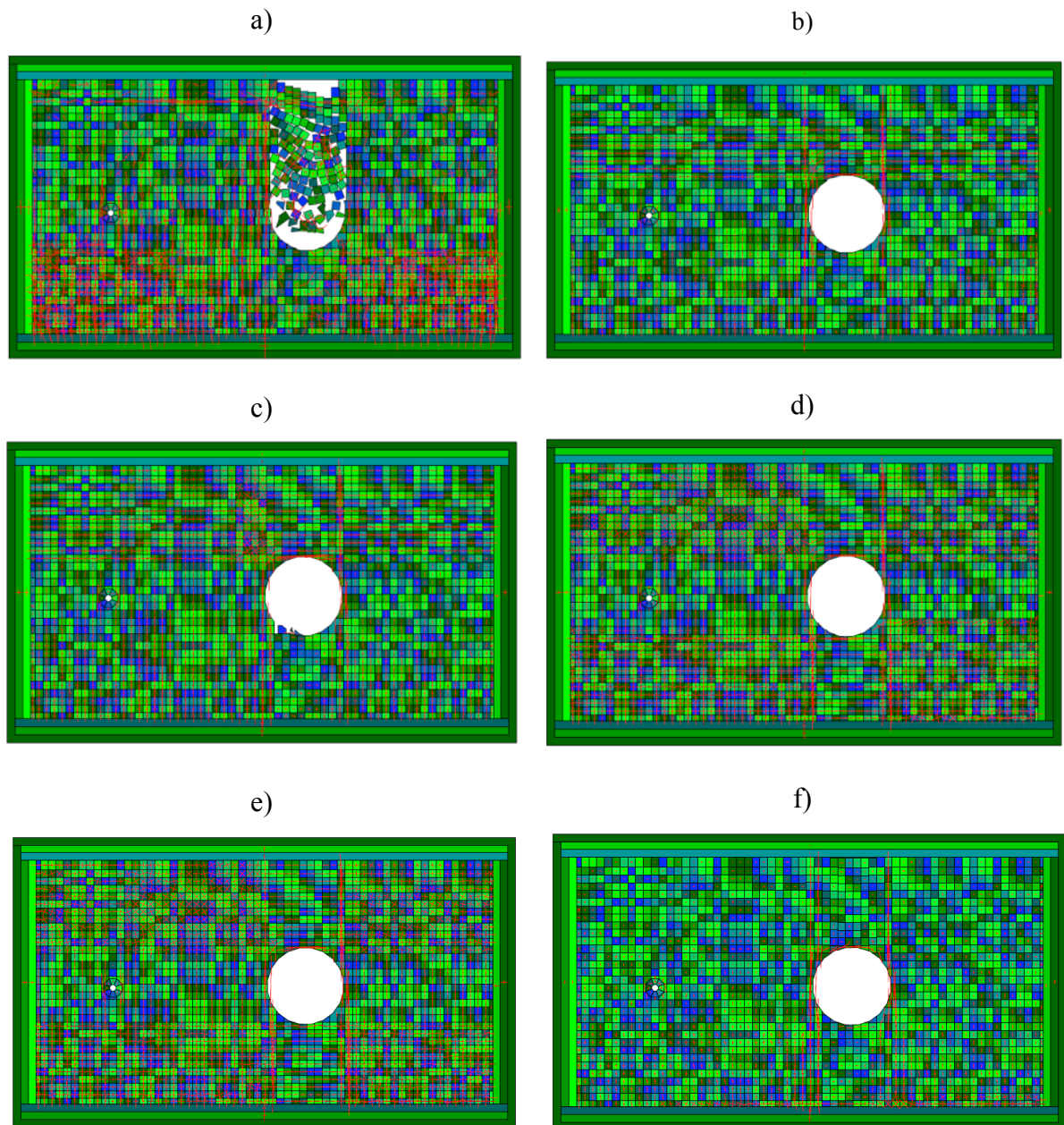


Figure 6.8 – Principal stress trajectories at the end of the DDA simulation with no initial stresses with joint friction angle of a) 0°, b) 5°, c) 15°, d) 25°, e) 35°, f) 45°.

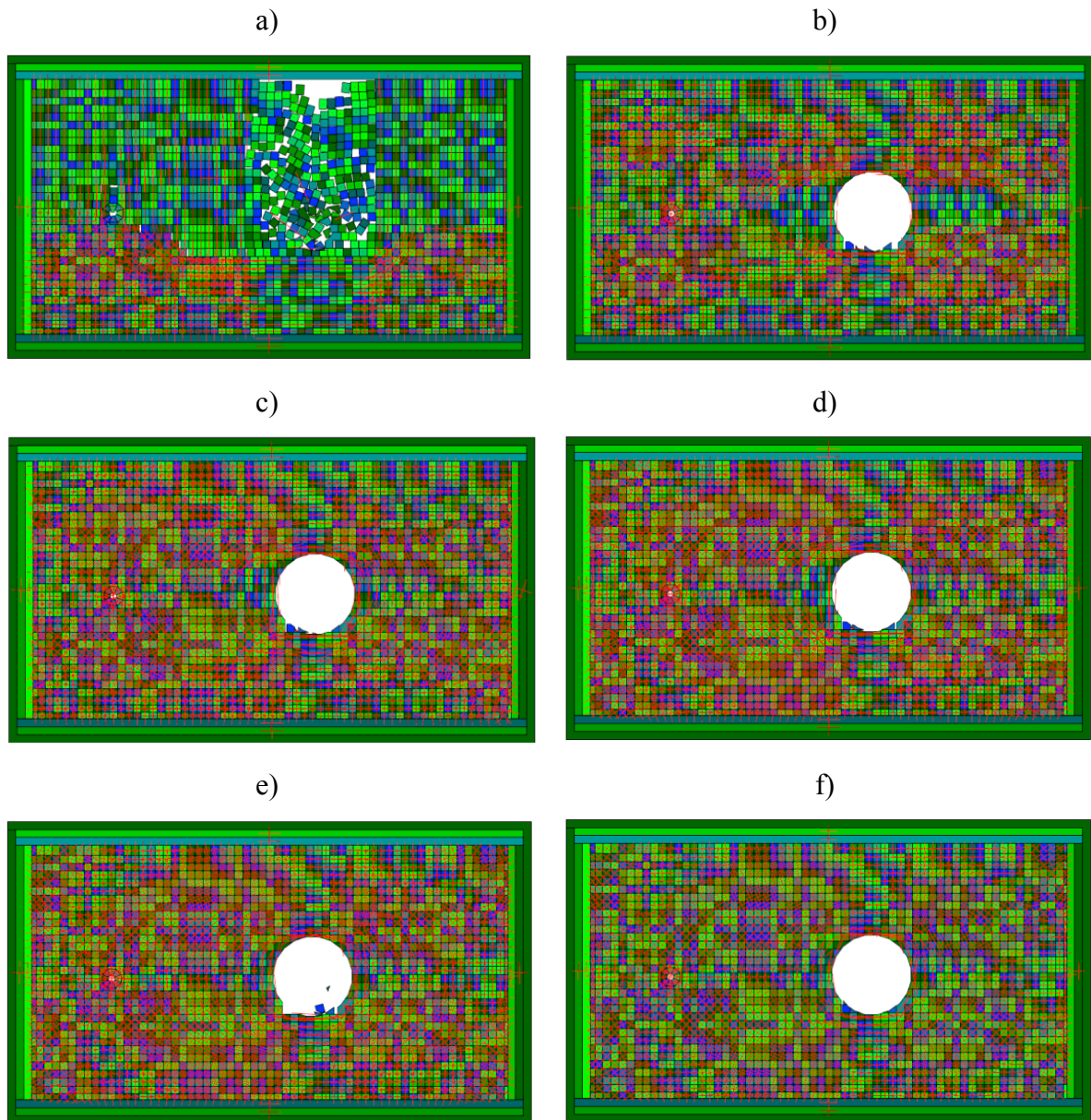


Figure 6.9 - Principal stress trajectories at the end of the simulation with initial hydrostatic stresses of 50 MPa with joint friction angles of a) 0° , b) 5° , c) 15° , d) 25° , e) 35° , f) 45°.

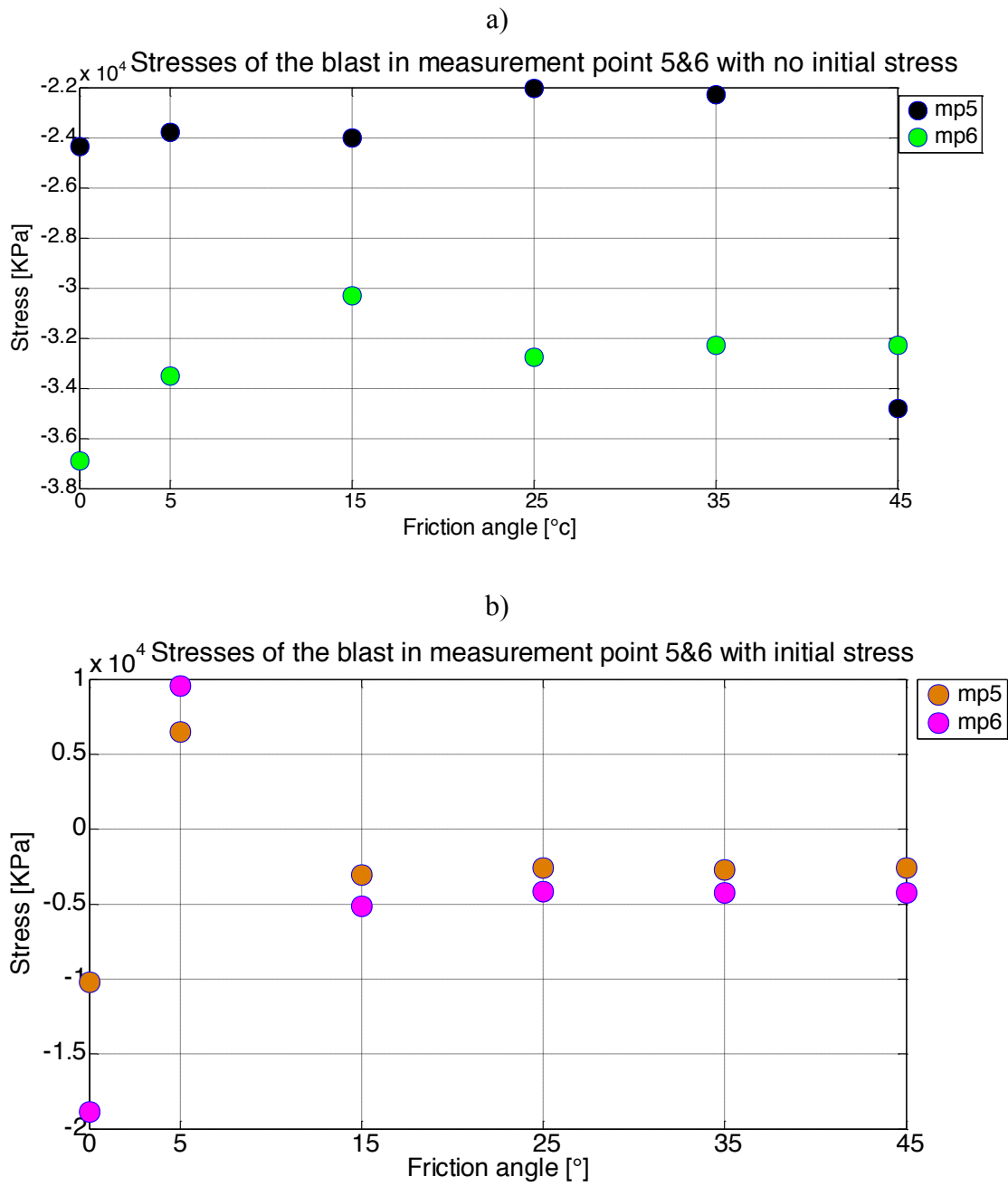


Figure 6.10 – Peak stress recorded in the control point 5 and 6 (a) without initial stress (b) with initial hydro stress of -50 MPa.

6.2.3 The effects of the friction angle and the initial stresses

We find that in general the structure remained stable for all friction angles, except for zero friction, where collapse occurred in the roof as indicated above. The peak velocity and acceleration at the four measurement points around the tunnel shown in Figure 6.11 indicate that points 1 and 2 exhibited the strongest response to the shock wave, at the sidewall and roof, respectively. In the simulation with no initial stresses, measurement point no.1 in the sidewall closer to the blast exhibited the highest peak particle velocity with every joint friction angle. However, when the medium was subjected to initial stresses, the strongest response was measured at point 2 in the roof for most values of joint friction.

It can be seen that the response of the sidewalls to the blast is greater with no initial stresses. This is best evident when examining the response of key-block no. 1 (Figure 6.12). As would be expected, peak velocity and accelerations are restrained in both scenarios with increasing frictional resistance on the joints. The initial stresses and the friction angle of the discontinuities stabilize the rock mass. Thus, in order to destabilize the system by displacing blocks, more energy is needed to overcome the initial stabilizing conditions of the initial stresses and friction.

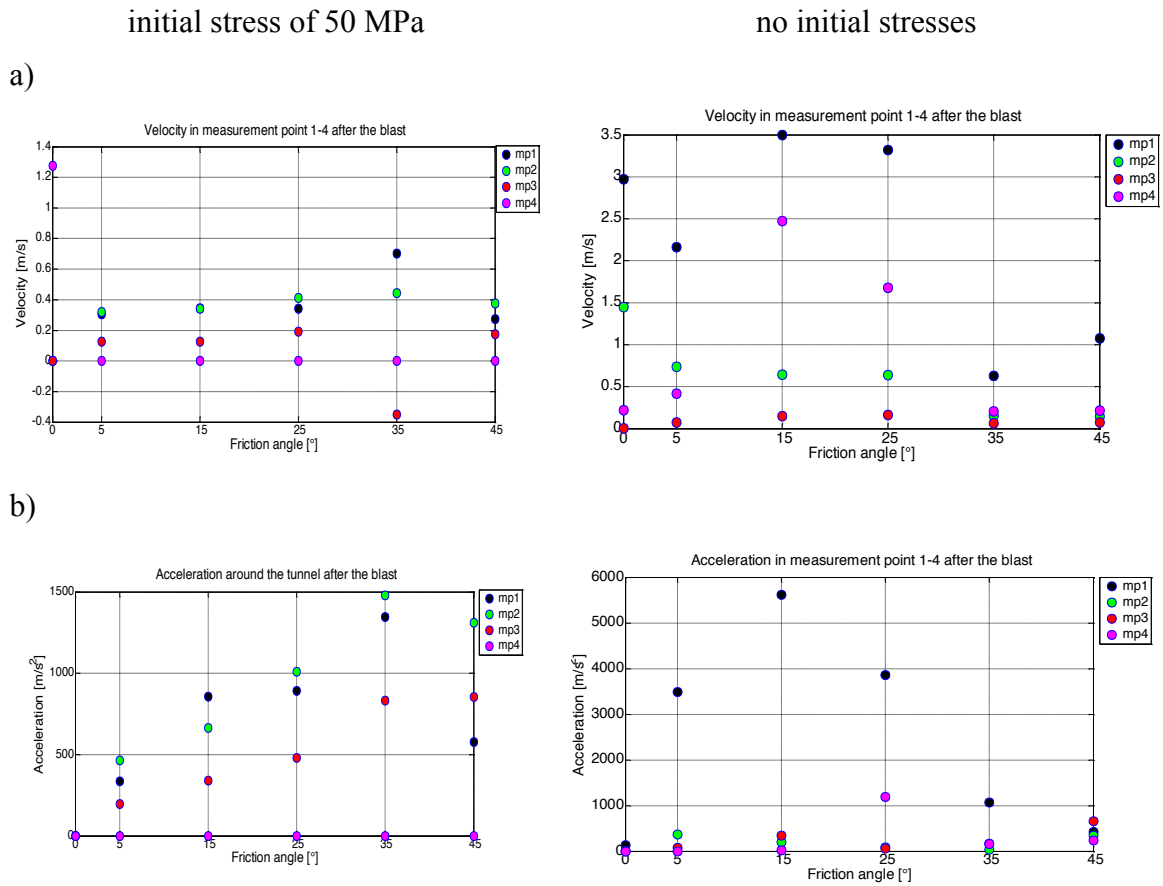


Figure 6.11- Peak velocity (a) and peak acceleration (b) around the tunnel with (left) and without (right) initial stresses.

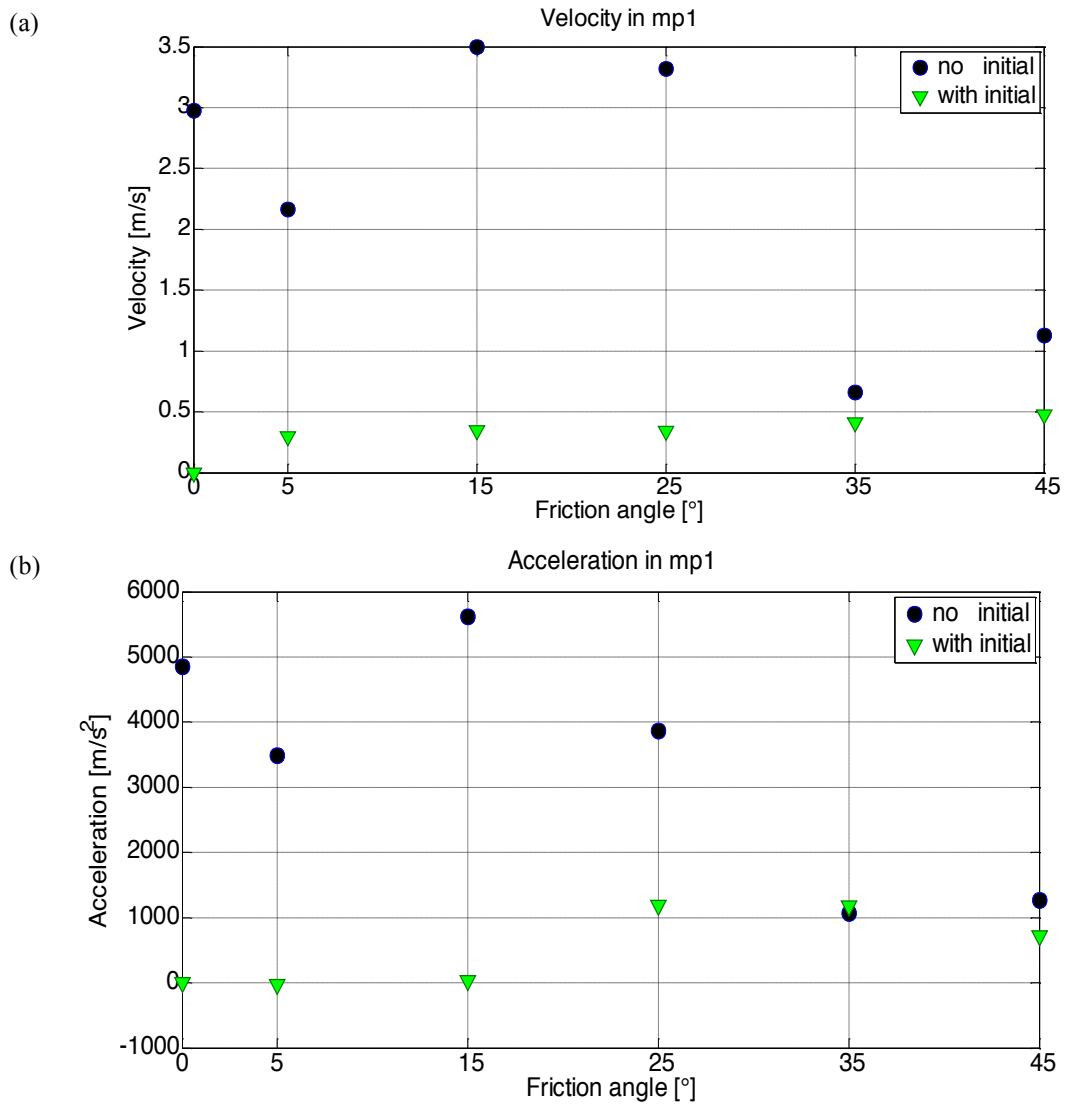


Figure 6.12- Peak velocity (a) and peak acceleration (b) of key-block 1 with initial hydrostatic stress of 0 MPa (Blue circles) and 50 MPa (Green triangles)

Chapter 7 - Summary and conclusions

The DDA method is used to study two rockburst triggering mechanisms: 1) strain relaxation in response to excavation, and 2) energy redistribution in response to blasting.

Two DDA enhancements are utilized in this research: 1) non reflective boundaries, and 2) sequence excavation modeling. The use of these enhancements in the simulations proved to be effective and allowed greater accuracy in acquiring more realistic results.

We find that P-wave arrival time and amplitude accuracy greatly depend upon the block length and time interval used in DDA. This also led us to develop a new blast model which produces radial P-wave propagation from the point source into the jointed domain. This new method adds a new function to the DDA that can be used to analyze rock stability and reaction in problems where blasting is practiced.

We find that strain relaxation may trigger rockbursts in tunnels excavated through discontinuous rock masses under high initial in-situ stresses. Blasting, on the other hand, when associated with nearby excavation activities may trigger rockbursts in discontinuous rock masses when the initial in-situ stress level is relatively low.

Further study in relation to the present results may include the energy dissipation associated with slip along joints once the opening is created to better understand the energy balance associated with rockbursts. Moreover, we suggest that a study of the effect of the distance between the blast source and the tunnel, and in different geometries may prove useful.

Bibliography

- Van den Abeele, K. et al., 2007. An accuracy and stability study of the 2D spectral volume method. *Journal of Computational Physics*, 226(1), pp.1007–26.
- Ainsworth, M. & Wajid, H.A., 2009. dispersive and dissparive behavior of the spectral element method. , 47(5), pp.3910–37.
- Bao, H., Hatzor, Y.H. & Huang, X., 2012. A New Viscous Boundary Condition in the Two-Dimensional Discontinuous Deformation Analysis Method for Wave Propagation Problems. *Rock Mechanics and Rock Engineering*, 45(5), pp.919–28.
- Brady, B.H.G. & Brown, E.T., 2007. *Rock mechanics: for underground mining* second, 19., Dordrecht: Chapman & Hall, London.
- Brady, B.T. & Leighton, F.W., 1977. Seismicity anomaly prior to a moderate rock burst: a case study. , 14(3), pp.127–32.
- Cai, M. et al., 2004. Generalized crack initiation and crack damage stress thresholds of brittle rock masses near underground excavations. *International Journal of Rock Mechanics and Mining Sciences*, 41(5), pp.833–47.
- Chang, C., 1994. Nonlinear dynamic discontinuous deformation analysis with finite element meshed block system.
- Chen, B.-R. et al., 2013. Rock Burst Intensity Classification Based on the Radiated Energy with Damage Intensity at Jinping II Hydropower Station, China. *Rock Mechanics and Rock Engineering*, 48(1), pp.289–303.
- Chen, G., 2003. Numerical Modelling of Rock Fall Using Extended Dda. , 22(6), pp.926–31.
- Chen, S. & Zhao, J., 1998. A study of UDEC modelling for blast wave propagation in jointed rock masses. *International Journal of Rock Mechanics and Mining*
- Cook, N.G.W., 1966. The basic mechanics of rockbursts. *Journal of the Southern African Institute of Mining and Metallurgy*, 66(3), pp.56–70.
- Doolin, D.M. & Sitar, N., 2004. Time Integration in Discontinuous Deformation Analysis. *Journal of Engineering Mechanics*, 130(3), pp.249–58.

- Durrheim, R. et al., 1998. Violent failure of a remnant in a deep South African gold mine. *Tectonophysics*, 289(1-3), pp.105–16.
- Feng, G., Feng, X. & Zhao, Z., 2013. Rockburst risk analysis based on MS monitoring in deep-buried tunnel with TBM excavation. In *3rd ISRM Symposium on Rock Characterisation, Modelling and Engineering Design Methods*. SINOROCK.
- Feng, G.-L. et al., 2015. Sectional velocity model for microseismic source location in tunnels. *Tunnelling and Underground Space Technology*, 45, pp.73–83.
- Feng, X.T. et al., 2012. Studies on the evolution process of rockbursts in deep tunnels. *Journal of Rock Mechanics and Geotechnical Engineering*, 4(4), pp.289–95.
- Gay, N.C. & Ortlepp, W.D., 1979. Anatomy of a mining-induced fault zone. *Geological Society of America bulletin*, 90(1), pp.47–58.
- Goodman, R. & Shi, G.-H., 1985. *Block theory and its application to rock engineering*, Englewood Cliffs, NJ: Prentice-Hall.
- Gu, R. & Ozbay, U., 2014. Distinct element analysis of unstable shear failure of rock discontinuities in underground mining conditions. *International Journal of Rock Mechanics and Mining Sciences*, 68, pp.44–54.
- Hatzor, Y.H., Wainshtein, I. & Bakun Mazor, D., 2010. Stability of shallow karstic caverns in blocky rock masses. *International Journal of Rock Mechanics and Mining Sciences*, 47(8), pp.1289–1303.
- He, M.C. et al., 2015. Rockburst laboratory tests database — Application of data mining techniques. *Engineering Geology*, 185, pp.116–30.
- Heal, D.P., 2010. *Observations and analysis of incidences of rockburst damage in underground mines*. Ph.D. Thesis, The University of Western Australia, Perth, Australia.
- Hsiung, S. & Shi, G.-H., 2001. Simulation of earthquake effects on underground excavations using discontinuous deformation analysis (DDA). In *DC Rocks 2001, The 38th US Symposium on Rock Mechanics (USRMS)*. American Rock Mechanics Association.
- Huang, R.Q., Wang, X.N. & Chan, L.S., 2001. Triaxial unloading test of rocks and its implication for rock burst. *Bulletin of Engineering Geology and the Environment*, 60(1), pp.37–41.
- Jing, L., Ma, Y. & Fang, Z., 2001. Modeling of fluid flow and solid deformation for fractured rocks with discontinuous deformation analysis (DDA) method. *International Journal of Rock Mechanics and Mining Sciences*, 38(3), pp.343–55.

- Kaiser, P.K. & Cai, M., 2012. Design of rock support system under rockburst condition. *Journal of Rock Mechanics and Geotechnical Engineering*, 2012(3), pp.215–27.
- Kaiser, P.K. & Maloney, S.M., 1997. Scaling laws for the design of rock support. *Pure and Applied Geophysics*, 150(3-4), pp.415–34.
- Kaiser, P.K., McCreath, D.R. & Tannant, D.D., 1996. *Canadian rockburst support handbook*, Geomechanics Research Centre, Laurentian University, Sudbury, Ontario.
- Kim, Y.-I., Amadei, B. & Pan, E., 1999. Modeling the effect of water, excavation sequence and rock reinforcement with discontinuous deformation analysis. *International Journal of Rock Mechanics and Mining Sciences*, 36(7), pp.949–70.
- Kolsky, H., 1964. Stress waves in solids. *Journal of Sound and Vibration*, 1(1), pp.88–110.
- Lee, S.M., Park, B.S. & Lee, S.W., 2004. Analysis of rockbursts that have occurred in a waterway tunnel in Korea. *International Journal of Rock Mechanics and Mining Sciences*, 41(SUPPL. 1), pp.1–6.
- Leet, L., 1951. Vibration studies; blasting and rock bursts. *Canadian Mining and Metallurgical Bulletin*, 470.54, pp.415–18.
- Li, S. et al., 2012. In situ monitoring of rockburst nucleation and evolution in the deeply buried tunnels of Jinping II hydropower station. *Engineering Geology*, 137-138(null), pp.85–96.
- Lin, C. et al., 1996. Extensions of Discontinuous s for Jointed Rock. *International Journal of Rock Mechanics and Mining Sciences*, 33(7), pp.671–94.
- Low, H., 2001. Reliability analysis of reinforced concrete slabs under explosive loading. *Structural Safety*, 23(2), pp.157–78.
- Lu, C.P. et al., 2013. Microseismic frequency-spectrum evolutionary rule of rockburst triggered by roof fall. *International Journal of Rock Mechanics and Mining Sciences*, 64, pp.6–16.
- Lysmer, J. & Kuhlemeyer, R.L., 1973. Wave propagation analysis of two-phase saturated porous media using coupled finite-infinite element method. *Journal of Soil Mechanics & Foundations Div*, 99(sm5), pp.421–27.
- MacLaughlin, M. & Sitar, N., 1999. A gravity turn-on routine for DDA. In *3rd International Conference on Analysis of Discontinuous Deformation (ICADD-3)*. ARMA, VAIL, CO, pp. 65–74.

- Mansurov, V. a., 2001. Prediction of rockbursts by analysis of induced seismicity data. *International Journal of Rock Mechanics and Mining Sciences*, 38(6), pp.893–901.
- Mitri, H., 1999. FE modelling of mining-induced energy release and storage rates. *J. Inst. Min. and Metall.*, 99(2), pp.103–10.
- Müller, W., 1991. Numerical simulation of rock bursts. *Mining Science and Technology*, 12(1), pp.27–42.
- Ohnishi, Y. & Nishiyama, S., 2005. The application of DDA to practical rock engineering problems: issues and recent insights. *Proceedings of Seventh*
- Ortlepp, W., 1978. The Mechanism Of A Rockburst. In *19th US Symposium on Rock Mechanics (USRMS)*. Reno: University of Nevada, pp. 476–83.
- Ortlepp, W.D. & Stacey, T.R., 1998. Performance of tunnel support under large deformation static and dynamic loading. *Tunnelling and Underground Space Technology*, 13(1), pp.15–21.
- Ortlepp, W.D. & Stacey, T.R., 1994. Rockburst mechanisms in tunnels and shafts. *Tunnelling and Underground Space Technology*, 9(1), pp.59–65.
- Pearce, C.J. et al., 2000. Computational aspects of the discontinuous deformation analysis framework for modelling concrete fracture. *Engineering Fracture Mechanics*, 65(2-3), pp.283–98.
- Rice, J.R., 1983. Constitutive relations for fault slip and earthquake instabilities. *Pure and Applied Geophysics PAGEOPH*, 121(3), pp.443–75.
- Rorke, A. & Roering, C., 1984. Source mechanism studies of mine-induced seismic events in a deep-level gold mine. In *1st Int. Congr. Rockbursts and Seismicity in Mines. S. Afr.* Johannesburg, pp. 51–55.
- Shi, G.-H., 1993. Block system modeling by Discontinuous Deformation Analysis C. A. Brebbia & J. . Connor, eds. *Topics in Engineering*, 11, p.209.
- Shi, G.-H., 1996. Discontinuous deformation analysis programs, version 96, user's manual. *RM-C. Young*, (June), p.25.
- Shi, G.-H., 1988. *Discontinuous deformation analysis: a new numerical model for the statics and dynamics of block systems*. University of California, Berkeley.
- Shi, G.-H. & Goodman, R.E., 1985. Two dimensional discontinuous deformation analysis. *International Journal for Numerical and Analytical Methods in Geomechanics*, 9(6), pp.541–56.
- Shiyong, W., Manbin, S. & Jian, W., 2010. Jinping hydropower project: main technical

- issues on engineering geology and rock mechanics. *Bulletin of Engineering Geology and the Environment*, 69(3), pp.325–32.
- Shyu, K., 1993. Nodal-based discontinuous deformation analysis.
- Spottiswoode, S., 1984. Source mechanisms of mine tremors at Blyvooruitzicht gold mine. *Rockbursts and Seismicity in Mines*, 6, pp.29–37.
- Srinivasan, C., Arora, S.K. & Yaji, R.K., 1997. Use of mining and seismological parameters as premonitors of rockbursts. *International Journal of Rock Mechanics and Mining Sciences*, 34(6), pp.1001–8.
- Tal, Y., Hatzor, Y.H. & Feng, X.-T., 2014. An improved numerical manifold method for simulation of sequential excavation in fractured rocks. *International Journal of Rock Mechanics and Mining Sciences*, 65, pp.116–28.
- US army engineers, 1972. Systematic Drilling and Blasting for Surface Excavations: Engineering Manual EM 1110—2—3800. *Office of Chief of Engineers, Washington, DC*, p.145.
- Wang, J.-A. & Park, H.D., 2001. Comprehensive prediction of rockburst based on analysis of strain energy in rocks. *Tunnelling and Underground Space Technology*, 16(1), pp.49–57.
- Wu, J.-H., Ohnishi, Y. & Nishiyama, S., 2004. Simulation of the mechanical behavior of inclined jointed rock masses during tunnel construction using Discontinuous Deformation Analysis (DDA). *International Journal of Rock Mechanics and Mining Sciences*, 41(5), pp.731–43.
- Xie, Y. & Li, T., 2004. Primary discussion on blast's affection on rock burst. *The Chinese Journal of Geological Hazard and Control*, 2004, 15.1, pp.61–64.
- Xu, Z. et al., 2003. Limitations of static load theory in rockburst research and preliminary analysis on dynamics Mechanism of rockburst. *Chinese Journal of Rock Mechanics and Engineering*, 22(8), p.2003.
- Yagoda-Biran, G., 2013. *Seismic Hazard Analysis Using the Numerical DDA Method*. Ben-Gurion University of the Negev.
- Yan, P. et al., 2015. Mitigation of rock burst events by blasting techniques during deep-tunnel excavation. *Engineering Geology*, 188, pp.126–36.
- Yeung, M. & Leong, L., 1997. Effects of joint attributes on tunnel stability. *International Journal of Rock Mechanics and Mining ...*, 34(348), pp.3–4.
- Zhang, C. et al., 2012. Case Histories of Four Extremely Intense Rockbursts in Deep

Tunnels. *Rock Mechanics and Rock Engineering*, 45(3), pp.275–88.

Zhang, Y. et al., 2014. Extension of discontinuous deformation analysis and application in cohesive-frictional slope analysis. *International Journal of Rock Mechanics and Mining Sciences*, 70, pp.533–45.

Zhao, X.G. et al., 2014. Influence of unloading rate on the strainburst characteristics of beishan granite under true-triaxial unloading conditions. *Rock Mechanics and Rock Engineering*, 47(2), pp.467–83.

Appendix A

Matlab code for input into dc code

```
clear;
clc;

[line_cord, layer]=xlsread('face+blast10\roundtun1+blast10.xls'); %
read the file of coordinates
[row,column]=size(layer);
a=[]; % mesh geometry matrix
b=[]; % boundary line matrix
ab=[]; % absorbing boundary line matrix
f=[]; % fix point matrix
l=[]; % loading point matrix
m=[]; % measurement point matrix
h=[]; % hole point matrix
r=[]; % point in the removed block matrix
% the next loops will sort the file 'coordinates' in to the different
% matrix
for i=2:row
    switch layer{i}
        case {'blast'}
            a=[a; line_cord(i-1, 1:4), 1];

        case {'boundary'}
            a=[a; line_cord(i-1, 1:4), 1];

        case {'rock'}
            a=[a; line_cord(i-1, 1:4), 1];

        case {'fix point'}
            f=[f; line_cord(i-1, 5:6), line_cord(i-1, 5:6)];

        case {'absorbing boundary'}
            ab=[ab; line_cord(i-1, 1:4)];
            a=[a; line_cord(i-1, 1:4), 1];

        case {'load point'}
            l=[l; line_cord(i-1, 5:6)];

        case {'hole point'}
            h=[h; line_cord(i-1, 5:6)];

        case {'measure point'}
            m=[m; line_cord(i-1, 5:6)];

        case {'tunnel'}
            a=[a; line_cord(i-1, 1:4), 1];

        case {'removable hole'}
            r=[r; line_cord(i-1, 5:6)];
```

```
        otherwise
            disp(layer(i));
    end

end

mesh=size(a,1);      %count the number of mesh lines
boundary=size(b,1); %count the number of boundary lines
material_line=0;    %count the number of material lines
bolt=0;             %count the bolts
fixd=size(f,1);    %count the fixed points
load=size(l,1);    %count the load points
measure=size(m,1); %count the measure points
hole=size(h,1);    %count the hole points
removed=size(r,1); %count the remove points

% writing the fc file
fid=fopen('dc_round+bR10.txt', 'wt'); % open file for writing
fprintf(fid, '%d \n', 0.001); % write to file minimum edge length
parameter
fprintf(fid, '%d %d \n', mesh+boundary , boundary); % write to file
total number of lines and boundry lines
fprintf(fid, '%d \n%d \n%d \n%d \n%d \n%d \n%d \n',
material_line,bolt,fixd,load,measure,hole,bolt,removed ); % write to
file number of the different points
fprintf(fid, '%d %d %d %d \n', a'); % write to file the mesh
geometry matrix
fprintf(fid, '%d %d %d %d \n', b'); % write to file the boundary
geometry matrix
fprintf(fid, '%d %d %d %d \n', f'); % write to file the fixed line
matrix
fprintf(fid, '%d %d \n', l'); % write to file the loading point matrix
fprintf(fid, '%d %d \n', m'); % write to file the measured point
matrix
fprintf(fid, '%d %d \n', h'); % write to file the hole point matrix
fprintf(fid, '%d %d \n', r'); % write to file the removed blocks
matrix
fprintf(fid, '%d %d \n%d \n', 1, 1 ,4); % write to file the wave
veloctiy reduction ratio and number of absorbing boundary lines
fprintf(fid, '%d %d %d %d \n', ab'); % write to file the absorbing
boundry matrix
fprintf(fid, '%d \n', 0.0); % write to file the number of traction
lines
fclose(fid);
```

תקציר

פיצוץ סלע ספונטניים מוגדרים בספרות כתנועה פתאומית של סלע אשר מתרחשת בעיקר בחפירות עמוקות ידי אדם. הפיצוצים יכולים להגיע לעוצמות שונות ואף לגרום לנזק משמעותי לחיי אדם וציוד. קיימים שני מנגנונים עיקריים להיווצרות פיצוצים אלו: (1) שחרור עיבורים אשר מוביל לתזוזות בפני השטח של המנהרה. (2) אנרגיה נוספת אשר נכנסת למערכת, בדרך כלל בשל פיצוצים שנעשים באזור הכרייה.

בעבודה זו אנו חוקרים את המנגנונים השונים להיווצרות פיצוץ הסלע באמצעות שימוש בשיטה ספרתית הנקראת DDA המיועדת לניתוח מעוות בתווך בלתי רציף. באמצעות שדרוגים לשיטה, שפותחו לאחרונה בקבוצת המחקר באוניברסיטת בן גוריון, קיימת היום האופציה לבצע שליפה בשלבים של מנהרה והוספת גבולות משככים למרחב המחושב. באמצעות תוספות אלו, אנו יכולים לפתור בעיות דינמיות בסביבת עומסים גבוהים בדיוק גבוה יותר מבעבר. המחקר מתמקד בבלוקים שמשחררים עקב החלקה על שברים קיימים ולא בבלוקים חדשים העשויים להיווצר עקב הפיצוץ, כיוון שאנו מניחים שעקב שחרור העיבורים בלוקים ברי תזוזה ישוחררו אל המנהרה לפני שהסלע הרציף יכנע.

תחילה, אימתנו את הדיוק של שיטת ה-DDA באמצעות חישוב התקדמות גל לחץ בקורה אלסטית חד-מימדית. התוצאות הראו כי ה-DDA אכן נותן דיוק גבוה כל עוד החישוב נעשה באמצעות פסיעות זמן קטנות מספיק. כמו כן מצאנו כי היחס הנדרש בין אורך הבלוקים במודל לאורך גל הנבדק על מנת להגיע לרמת דיוק גבוהה בפתרון הוא בין $1/8$ ל- $1/12$. לאחר מכן המשכנו בפיתוח מודל חדש של התקדמות גלים רדיאלית המדמה פיצוץ. איששנו את יכולותיו של מודל הפיצוץ החדש באמצעות השוואה לתוצאות חיישנים ממקרה של פיצוץ בסלע אשר אירע בפרויקט מנהור הקשור לבניית תחנה הידרואולית תחת עומק גבוה של כ-2500 מ'.

לאחר ביצוע הבדיקות בהצלחה, ביצענו הדמיות של שני המנגנונים אשר יוצרים את הפיצוצים הספונטניים: (1) שחרור עיבורים כתוצאה מיצירת מנהרה תחת מאמצים ראשוניים משתנים (0-50 מגה פסקל), ו- (2) כתוצאה מפיצוצים בקרבת המנהרה, שנבדקו במסות סלע בלתי רציף עם זוויות חיכוך משתנות ומאמצים ראשוניים שונים. מצאנו שישנו קשר הדוק בין המאמצים ההתחלתיים למהירות ולתאוצה של הבלוק שנשלף במהלך הפיצוץ. בנוסף מצאנו כי ההשפעה של הפיצוץ המבוקר על הפיצוץ הספונטני גדלה כאשר המאמצים ההתחלתיים קטנים. מכאן הסקנו כי תחת מאמצים ראשוניים נמוכים ישנה השפעה גדולה יותר של פיצוצים סמוכים על יציבות המנהרה. לעומת זאת, תחת מאמצים ראשוניים גבוהים, כלומר ככל שמעמיקים, להוצאת המנהרה ושחרור העיבורים ישנו תפקיד מכריע בהיווצרות פיצוצים ספונטניים במנהרה.

אוניברסיטת בן-גוריון בנגב

הפקולטה למדעי הטבע
המחלקה למדעי הגיאולוגיה והסביבה

מידול התפוצצויות סלעים ספונטניות בסלע באמצעות

השיטה הנומריית DDA

חיבור זה מהווה חלק מהדרישות לקבלת התואר "מוסמך למדעי טבע (M.Sc.)"

מאת רוית זליג

בהנחיית פרופ' יוסף חודרה חצור

חתימת הסטודנט: _____ תאריך _____:

חתימת המנחה: _____ תאריך _____: *! חש*

חתימת יו"ר הועדה המחלקתית: _____ תאריך _____:

אוקטובר 2015

תשרי, התשע"ו



אוניברסיטת בן-גוריון בנגב
Ben-Gurion University
of the Negev

הפקולטה למדעי הטבע
The Faculty of Natural Sciences
המחלקה למדעי הגיאולוגיה והסביבה
Department of Geological &
Environmental Sciences

מידול התפוצצויות סלעים ספונטניות בסלע באמצעות השיטה הנומרית DDA

חיבור זה מהווה חלק מהדרישות לקבלת התואר "מוסמך למדעי טבע (M.Sc.)"

מאת: רות זליג

בהנחיית פרופ' יוסף חודרה הצור

אוקטובר 2015

תשרי, התשע"ו